VGA PROJECTION DISPLAY USING ELECTROMAGNETICALLY ACTUATED STEEL MICROMIRRORS

by

Mehmet Usta

B.S., Electrical and Electronics Engineering, Boğaziçi University, 2008

Submitted to the Institute for Graduate Studies in
Science and Engineering in partial fulfillment of
the requirements for the degree of
Master of Science

Graduate Program in Electrical and Electronics Engineering
Boğaziçi University
2011

ACKNOWLEDGEMENTS

I would like to express my utmost gratitude to my thesis supervisor Prof. Şenol Mutlu for his guidance and support. He is the person who introduced me to MEMS based projection display technology. I am grateful to Prof. Arda Deniz Yalçınkaya for his contributions and guidance. He has never hesitated to share his knowledge and time. I would like to sincerely thank Prof. Arda Yurdakul for her valuable guiding comments on my thesis and for kindly taking part in my thesis jury.

I owe my deepest gratitude to my immediate manager retired navy captain Muharrem Demirbaş for his endless support and unquestioned trust. He is a person who has worked for his country throughout his life. I would like to also thank all the managers and employees of TUBİTAK UEKAE. This thesis would not have been possible without the opportunities they provide. It is my pleasure to thank my colleagues Levent Balamir Tavacıoğlu, İsmail Camalan, Murat Akgül, and Onur Keskin for their sincere friendship and support.

I would like to particularly thank my colleague Selami Şahin for his valuable support in circuit design and realization. My special thank goes to my truehearted friend Soner Işıksal who has spared no effort in the course of accomplishment of my thesis.

I would like to also thank my parents-in-law, Ayla and Namık Küçükakarsu, for supporting me in every way they can. I would like to express my gratitude to my beloved parents Emine and Mehmet Usta who have raised me with care and love. In every stage of my life, they have always supported me in the most sincere way with no expectation.

Finally, the most important thank goes to my wife Betül Küçükakarsu Usta who always cares for me much more than I do. I have felt her support and diligence throughout every stage of my master's study.

ABSTRACT

VGA PROJECTION DISPLAY USING ELECTROMAGNETICALLY ACTUATED STEEL MICROMIRRORS

Projection display in VGA display format, which is 640x480 pixels in resolution, is aimed to be achieved using electromagnetically actuated steel micromirrors. In the work, the focus is the projection display control system but not the micromirrors. A projection control system, which is capable to control the actuation of the micromirror whose specifications meet the VGA display format requirements, is designed, simulated and realized. The projection control system is capable to generate a superimposed current signal consisting of sinusoidal signal at frequency of 16 kHz and saw-tooth signal at frequency of 60 Hz and it can modulate the laser at frequency of 18.5 MHz to form an image in VGA resolution. Micromirror actuation is controlled by controlling the actuating electro-coil current. In order to control the coil current, linear closed loop current control technique with four-quadrant non-simultaneous complementary PWM switching is used. Simulation of the closed loop current control is done for signals in different waveforms and at different frequencies. Realization of the projection display control system is based on a digital signal controller. Closed loop current control algorithm runs on the digital signal controller. Modulation of the laser is also done with the digital signal controller. The steel micromirror used in the work does not meet the VGA display format requirements but it is the scanner whose performance is the closest to VGA requirements among the micromirrors we have. The fast scan frequency of the micromirror is 11271 Hz and the slow scan frequency is 285 Hz. The projection display control system is adjusted to work with this micromirror. Experiments were done with the control system and the micromirror. Images with 20x40 resolution in pixels were achieved as the results of the experiments.

ÖZET

ELEKTROMANYETİK YÖNTEMLE HAREKETİ SAĞLANAN ÇELİK MİKRO AYNALARLA OLUŞTURULAN VGA PROJEKSİYON GÖRÜNTÜ

Bu çalışmada, VGA özelliklerine sahip bir projeksiyon görüntü elektromanyetik yöntemle hareket ettirilen mikro ayna kullanılarak oluşturulmaya çalışılmıştır. VGA görüntü 640x480 çözünürlüğe sahiptir. Çalışma sırasında projeksiyon görüntü kontrol sistemi tasarımı ve gerçeklenmesi üzerine yoğunlaşılmış olup mikro ayna tasarımı ve üretimi üzerine herhangi bir çalışma yapılmamıştır. VGA görüntü isterlerini karşılayabilen mikro aynaların hareket kontrolünü yapabilen bir projeksiyon kontrol sistemi tasarlanmış, benzetimi yapılmış ve gerçeklenmiştir. Projeksiyon görüntü kontrol sistemi VGA çözünürlükte görüntü elde etmek için 16 kHz sinüs sinyalinin ve 60 Hz üçgen sinyalinin toplamından oluşan akım sinyalini oluşturabilmekte ve 18.5 MHz frekans değerinde lazer kiplemesi yapabilmektedir. Mikro ayna hareket kontrolü hareketi sağlayan bobinin akımının kontrolüyle sağlanmaktadır. Bobin akımının kontrolü için kapalı çevrim doğrusal akım kontrol tekniği kullanılmıştır. Bu akım kontrol tekniği dört zamanlı tamamlayıcı PWM anahtarlamayı kullanmaktadır. Kapalı çevrim akım kontrolünün farklı frekansta ve biçimde sinyaller için benzetimi yapılmıştır. Projeksiyon kontrol sistemi bir sayısal sinyal kontrolcü kullanılarak gerçeklenmiştir. Sayısal sinyal kontrolcü kapalı çevrim akım kontrol algoritmasını koşturmaktadır ve lazer kiplemesini yapmaktadır. Bu çalışmada kullanılan çelik mikro ayna VGA görüntü isterlerini karşılamamaktadır ancak elimizde bulunan mikro aynalar içerisinde VGA görüntü isterlerini karşılamaya en yakın mikro aynadır. Kullanılan çelik aynanın hızlı tarama frekansı 11271 Hz yavaş tarama frekansı ise 285 Hz dir. Projeksiyon kontrol sistemi bu çelik ayna ile çalışabilecek şekilde ayarlanmış ve deneyler yapılmıştır. Deneyler sonucunda 20x40 çözünürlüğe sahip projeksiyon görüntüler elde edilmiştir.

TABLE OF CONTENTS

ACKNOWLEDGEMENTS iii
ABSTRACT iv
ÖZET v
LIST OF FIGURES viii
LIST OF TABLES xii
LIST OF SYMBOLS xiii
LIST OF ABBREVIATIONS xiv
1. INTRODUCTION 1
1.1. Micromirror Scanners 1
1.2. Micromirror Based Projection Display 3
1.2.1. VGA Display Projection 6
1.3. Electromagnetic Actuation 6
1.4. Main Contrubitions and Outline 7
2. SYSTEM DESCRIPTION 9
2.1. General Description 9
2.2. Closed Loop Current Control 9
2.3. Current Sensing 14
2.4. Power Inverter 16
2.5. Laser Modulator 22
2.6. Simulation 22
3. SYSTEM IMPLEMENTATION 29
3.1. Hardware Implementation 29
3.1.1. Main Control Unit 32
3.1.2. Current Sense Circuitry 33
3.1.3. Power Inverter 34
3.1.4. Laser Modulation 34
3.1.5. Power Supplies 34
3.2. Firmware Implementation 35

3.2.1. Firmware Program Flow 35
3.2.2. Firmware Program Timing 40
4. EXPERIMENTS AND RESULTS 42
5. CONCLUSION 49
APPENDIX A: SIMULATION 51
APPENDIX B: IMPLEMENTATION 60
REFERENCES 66

LIST OF FIGURES

Figure 1.1. One dimensional micromirror scanner. 2

Figure 1.2. Two dimensional micromirror scanner. 2

Figure 1.3. Simple electrostatic actuator. 4

Figure 1.4. Micromirror scanning types. 5

Figure 1.5. Electromagnetic actuation: (a) micromirror structure; (b) actuation principle. 7

Figure 2.1. Projection display control system block diagram. 10

Figure 2.2. Closed loop current control block diagram. 13

Figure 2.3. Low-side current sense block diagram. 15

Figure 2.4. High-side current sense block diagram. 15

Figure 2.5. Bi-directional current sense block diagram. 16

Figure 2.6. Power inverter block diagram. 17

Figure 2.7. Sinusoidal PWM generation. (a) comparison of reference signal with triangle wave. (b) voltage between leg A and ground. (c) voltage between leg B and ground. (d) voltage between leg A and B. 19

Figure 2.8. PWM modulation method used in the system. (a) comparison of reference signal with triangle wave. (b) voltage at leg A. (c) voltage at leg B. (d) load voltage and current. 21

Figure 2.9. Voltage between leg A and ground. 25

Figure 2.10. Voltage between leg B and ground. 25

Figure 2.11. Voltage between the nodes of the sense resistor 1. 26

Figure 2.12. Voltage between the nodes of the sense resistor 2. 26

Figure 2.13. Voltage between the nodes of the load. 27

Figure 2.14. Load current in sinusoidal waveform with 300 usec simulation duration. 27

Figure 2.15. Load current in sinusoidal waveform with 1 msec simulation duration. 28

Figure 2.16. Superimposed load current consisting of high frequency sinusoidal and low frequency saw-tooth signals. 28

Figure 3.1. F2808 experimner kit from Texas Instruments [1]. 30

Figure 3.2. Original two layer power board. 31

Figure 3.3. System hardware; experimenter kit and power board together. . . 31

Figure 3.4. Firmware program flow block diagram. 36

Figure 3.5. First part of the interrupt routine pseudocode. 38

Figure 3.6. Second part of the interrupt routine pseudocode. 39

Figure 3.7. Firmware timing diagram. 41

Figure 4.1. Steel micromirror scanner attached on a holder. 42

Figure 4.2. Experimental setup. 43

Figure 4.3. Current sense waveforms. 44

Figure 4.4. Fast scan current signal in sinusoidal waveform. 45

Figure 4.5. Superimposed current signal consisting of high frequency sinusoidal and low frequency saw-tooth signals. 45

Figure 4.6. 2D raster scan with height of 6 cm and width of 12.5 cm. 46

Figure 4.7. 2D raster scan with height of 7 cm and width of 10 cm. 47

Figure 4.8. First image on the projection display. 47

Figure 4.9. Second image on the projection display. 48

Figure A.1. First part of the initialization function. 51

Figure A.2. Second part of the initialization function. 52

Figure A.3. PWM generator function. 53

Figure A.4. Complementary PWM generator function. 54

Figure A.5. PWM modulator function. 55

Figure A.6. First part of the PI controller function. 56

Figure A.7. Second part of the PI controller function. 57

Figure A.8. Simulation model. 58

Figure A.9. PWM generator model. 59

Figure B.1. First part of the interrupt routine. 60

Figure B.2. Second part of the interrupt routine. 61

Figure B.3. Third part of the interrupt routine. 62

Figure B.4. Power inverter schematic. 63

Figure B.5. Current sense circuitry schematic. 64

Figure B.6. Power supply schematic. 65

LIST OF TABLES

Table 1.1. Specifications of various display formats and requirements to achieve them. 5

Table 2.1. Parameters of the components of the system and their values. . . . 23

LIST OF SYMBOLS

C	Capacitance
c_{max}	Maximum Count Value
D	Scan Mirror Size
$e(k)$	Error at Time k
F	Actuating Force
f_c	Cut-off Freqeuncy of the Filter
f_f	Fast Scan Frequency
f_{op}	Operating Frequency
f_s	Switching Frequency
$F(\omega)$	Frequency Dependent Actuating Force
G_{cs}	Gain of the Current Sensing Circuitry
$H(\omega)$	Frequency Dependent H-field
$I(\omega)$	Frequency Dependent Current
K_I	Integral Gain
K_P	Proportional Gain
l	Length of Solenoid Coil
M	Magnetization Vector
N	Total Number of Turns of Solenoid Coil
t	Thickness of the Movable Frame
U_E	Stored Energy
$U_I(k)$	Integral Part of the Controller Output at Time k
$U_P(k)$	Proportional Part of the Controller Output at Time k
V	Applied Voltage
V_{SIG}	Voltage Value of the Signal
W	Width of the Movable Frame
θ	Maximum Scan Angle

LIST OF ABBREVIATIONS

1D	One Dimensional
2D	Two Dimensional
AC	Alternating Current
ADC	Analog to Digital Converter
CPU	Central Processing Unit
EDM	Electrical Discharge Machining
ePWM	Enhanced Pulse Width Modulation
GPIO	General Purpose Input Output
LCD	Liquid Crystal Display
LED	Light Emitting Diode
MOSFET	Metal Oxide Semiconductor Field Effect Transistor
MSPS	Million Samples Per Second
PCB	Printed Circuit Board
PI	Proportional and Integral
PWM	Pulse Width Modulation
SARAM	Single Access Random Access Memory
SOC	Start of Conversion
TOSA	Total Optical Scan Angle
TV	Television
USB	Universal Serial Bus
VGA	Video Graphics Array

1. INTRODUCTION

Display technology has developed rapidly since the first display was obtained by means of cathode ray tube. Today, it is in an exciting phase with LCD TVs, plasma TVs, LED LCD TVs, etc. Allocation of huge money and research resources on the development of display technologies may be explained by the huge market demand. Projection display is a strong alternative to TV and monitor. It has advantages over TVs and monitors in terms of form factor and ease in usage. While the monitors are getting thinner, projection devices are getting smaller and smaller. Projection display devices using optical scanners have been reaching the minimal form factor by MEMS technology. MEMS technology enables manufacturing of micro scale optical scanners at affordable costs. Most of the micro scale optical scanners used in display technology use micromirrors for their operation.

1.1. Micromirror Scanners

Optical scanner directs a beam of light in different directions in order to control the spatial position of that light beam. It achieves this by modifying the angular position of the incident beam rather than by changing the position of the ligth source. An optical micromirror scanner used in display systems consists of a light source and an articulated mirror. In general, a commercial laser diode packaged with a collimator lens is used as the light source.

Continuous optical scanning can be achieved by vibrating a micromirror in resonance. When the micromirror is tilted by an angle θ, the reflected light on the mirror is deflected by an angle 2θ. Therefore, the magnitude of the scanning angle is directly proportional to the mirror deflection amplitude. Vibrating the micromirror in resonance yields maximum deflection.

One dimensional tilting micromirror is the most common building block for optical scanning systems. It consists of a movable frame and two suspensions, which

are clamped to a stiff support. These suspensions act as torsional springs and give micromirror an angular degree of freedom. A 1D micromirror scanner is shown in Figure 1.1.

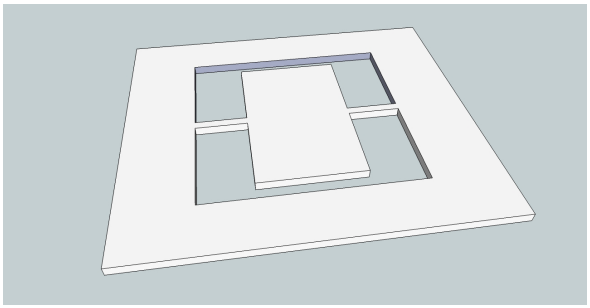

Figure 1.1. One dimensional micromirror scanner.

Two dimensional micromirror scanner with gimballed torsional structure has two orthonal torsional vibration modes, which give the micromirror two angular degree of freedom [2]. A 2D micromirror scanner with gimballed torsional structure is shown in Figure 1.2. This micromirror has two movable frames. The inner frame rotates about the fast scan axis and generates horizontal scan. The outer frame rotates about the slow scan axis and generates vertical scan. Both of the frames are excited at their resonance frequencies with a superimposed AC signal to achieve 2D raster scan. In this work, this kind of micromirror scanner is used.

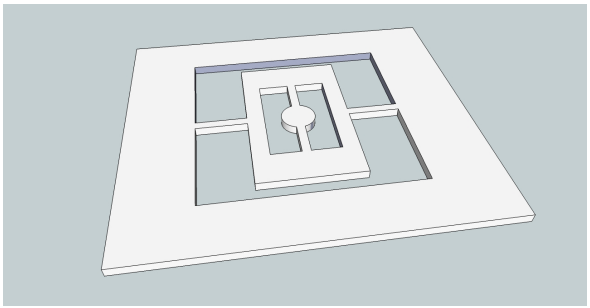

Figure 1.2. Two dimensional micromirror scanner.

1.2. Micromirror Based Projection Display

Using a 2D micromirror scanner with gimballed torsional structure, a projection display in different resolutions can be achieved. Each of the movable frames of the micromirror can be actuated in one axis so that the reflected ligth beam makes a 2D raster scan. Displacement of the inner frame generates horizontal scan and displacement of the outer frame generates vertical scan. There are four different most common actuation methods, which are electrostatic actuation, thermal actuation, piezoelectric actuation and electromagnetic actuation. These actuation methods are explained briefly.

Electrostatic actuation technique uses coulombic attraction force between two oppositely charged bodies. A simple capacitive electrostatic actuator is depicted in Figure 1.3. The electrostatic force, which actuates the micromirror, can be calculated from the stored energy.

$$U_E = \frac{1}{2} C V^2 \tag{1.1}$$

where C is the total capacitance and V is the applied voltage.

Then the electrostatic force is

$$F = \frac{\partial U_E}{\partial x} = \frac{1}{2} \frac{dC}{dx} V^2 \tag{1.2}$$

Electrostatic actuation requires high actuation voltage but has the advantage of implementiton simplicity.

There are micromirrors actuated by electrostatic actuators. Two of them are reported in [3] and [4].

Thermal actuation utilizes the termal expansion of metarials. A thermal actuator

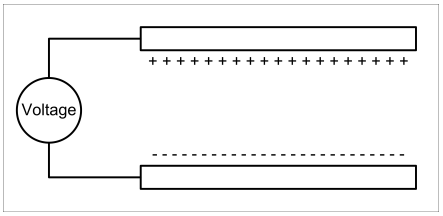

Figure 1.3. Simple electrostatic actuator.

consists of two materials with different thermal expansion coefficients which are put together as a bimorph structure. Thermal actuation can yield large rotation angles but has the disadvantages of thermal noise sensitivity and high response time. Thermal actuation is used in some applications [5] [6].

Piezoelectric actuation technique uses the piezoelectric transducer effect between electrical and mechanical oscillations. It yields precise actuation but has the disadvantage of low displacement. There are microscanners actuated by piezoelectric actuators [7].

Electromagnetic actuation uses electromagnetic force created by a current carrying coil to actuate the micromirror which is placed in a constant magnetic field. Electromagnetic actuation is used in this work and it will be explained in detail in Section 1.3

Actuating the inner and outer frames of the micromirror at their mechanical resonance frequencies yields maximum scan angle. Thus, micromirrors are actuated at their resonance frequencies in order to achieve maximum performance.

In addition to generation of 2D raster scan, light beam is modulated to create an image. In modulation, light source is turned on or off so that the reflected beam creates a visual effect on the spatial position of that beam according to the image desired to be formed. Modulation is dependent on the scanning type, which could be unidirectional

and bidirectional. In unidirectional scanning, modulation is done only during the forward sweep of the horizontal scanner whereas in bidirectional scanning, modulation is done in both scan directions. Bidirectional scanning doubles the horizontal scan lines but it requires modulation in reverse order during backward sweep of the horizontal scanner. Unidirectional and bidirectional scanning is illustrated in Figure 1.4.

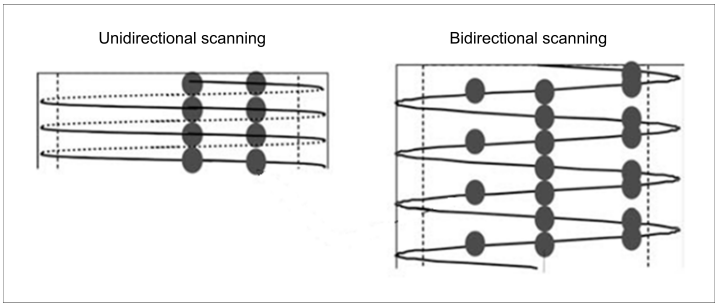

Figure 1.4. Micromirror scanning types.

The resolution of the projection display is dependent on the product θD and the scanner frequency. θ is the maximum mechanical scan angle amplitude and D is the scan mirror size. Product θD and scanner frequency requirements for various display formats are given in Table 1.1 [8].

Table 1.1. Requirements for various display formats.

Display Format	**Horizontal Resolution**	**Vertical Resolution**	θD **(deg.mm)**	**Fast Scan Freq. (Hz)**
QVGA	320	240	3.9	8000
VGA	640	480	7.8	16000
SVGA	800	600	9.7	20000
XGA	1024	768	12.4	256000
SXGA	1280	1024	15.6	34133
UXGA	1600	1200	19.4	40000
HDTV	1920	1080	23.3	36000

1.2.1. VGA Display Projection

In this work, it is aimed to achieve display projection in VGA format using micromirror scanners. As seen in Table 1.1, VGA display format has the horizontal resolution of 640 pixels and vertical resolution of 480 pixels. Using bidirectional scanning, for VGA resolution the micromirror scanner is required to have the fast scan frequency of 16000 Hz and the slow scan frequency of 60 Hz. The number of resolvable spots depends on the product θD. For VGA resolution, required prodcut θD is 7.8 with the frequencies given above.

1.3. Electromagnetic Actuation

Electromagnetic actuation utilizes the electromagnetic force to actuate the micromirror. It is current-based and has the advantages that it can generate both attractive and repulsive forces and it can achieve large displacement and force.

In Electromagnetic actuation, there are two sources, which are current carrying coil and a permanent magnet, to generate the magnetic field. Constant magnetic field is created by the permanent magnets put on two sides of the micromirror. The operation of electromagnetic actuation is depicted in Figure 1.5. When a current is passed through the coil, it generates H-field and electromagnetic force is excerted on the micromirror. Electromagnetic actuation forces generate out-of-plane displacements on the movable parts of the micromirror. Using the concentrated lumped loads at point 1 and at point 2, the induced forces on the movable parts can be approximated as [9]

$$F(\omega) = MWtH(\omega) \tag{1.3}$$

where M is the magnetization vector, W and t are the width and the thickness of the movable part. Frequency varying electromagnetic field vector $H(\omega)$, is dependent on

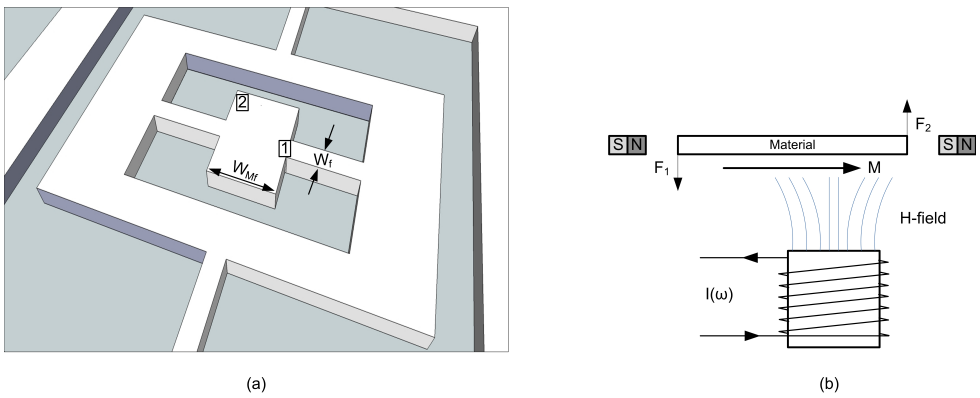

Figure 1.5. Electromagnetic actuation: (a) micromirror structure; (b) actuation principle.

the driving current of the coil. H-field of a solenoid coil is expressed as

$$H(\omega) = \frac{NI(\omega)}{l} \tag{1.4}$$

where N is the total number of turns and l is the length of the solenoid coil.

$I(\omega)$ is the actuating current, which is composed of two current signals. One component of the actuating current signal is in sinusoidal waveform and at fast scan frequency. The other component is in saw-tooth waveform and at slow scan frequency. Driving the coil with this superimposed current signal forces the micromirror to generate 2D raster scan.

There are numerous implementation of electromagnetic actuation in literature. Some of them are reported in [10–12].

1.4. Main Contrubitions and Outline

In this thesis, it is aimed to achieve VGA projection display using electromagnetically actuated micromirrors. The focus of the work is to design and realize the

projection display control system but not to design or fabricate the micromirror. The micromirror, reported in [13] is used in the work.

The material of the micromirror used in the work is steel. It is fabricated with EDM and electroplated with Nickel which is also a ferromagnetic material as steel. The fast scan frequency of the micromirror is 11271 Hz and the slow scan frequency is 285 Hz. These scan frequencies do not meet the VGA display format requirements but this micromirror is the scanner whose performance is the closest to VGA requirements among the fabricated micromirrors so far.

The projection control system is the system which controls the actuation of the micromirror and the modulation of the laser. Projection control system, which is capable to control the actuation of the micromirror whose scan frequencies meet the VGA requirements, is designed, simulated and realized. The system is also capable to modulate the laser to form an image in VGA resolution. Experiments were done with the realized system and the aforementioned micromirror. Results of the experiments are quite successfull with 20x40 resolution in pixels.

In the following chapter, the projection display control system is described in general and the components of the system is explained in detail. Simulation of the system is described and the results of the simulation is also given in the following chapter.

In Chapter 3, system implementation is explained in two parts, which are hardware implementation and firmware implementation.

In Chapter 4, experiments done with the system and the micromirror is decribed and results of the experiments are given.

In the last chapter, comments on the work are made and the works that may be done in the future are explained.

2. SYSTEM DESCRIPTION

2.1. General Description

"System" refers to electromagnetic actuation and laser modulation control system. As a more general statement, it can also be called projection display control system. For simplicity, only "system" will be used at the rest of the document.

System is based on closed loop current control of the actuation coil. It consists of main processing unit, current sensing, and power inverter and laser modulator. Main processing unit is responsible to run closed loop current control algorithm. Current sensing is responsible to provide feedback to the closed loop control system. Power inverter is responsible to generate AC signal in the form of required waveform. Main processing unit takes the measurements from current sensing as feedback and controls the power inverter with the means of chopping. When the current signal in the required waveform is applied to the actuation coil, 2-D raster scan is obtained. Laser modulator is responsible to modulate laser in order to form the 2-D raster scan image. A general block diagram of the system is shown in Figure 2.1. Closed loop current control, current sensing, power inverter and laser modulator will be explained in detail in the following sections.

2.2. Closed Loop Current Control

Equation 1.3 states that the electromagnetic force that the actuation coil produces is directly related to the current passing through it. Furthermore, it is a fact that there is a lag between the current and the voltage of a coil. All of these imply that controlling the voltage of a coil does not yield the direct control of the electromagnetic force but controlling the current of the coil yields direct control of the electromagnetic force. However, open loop current control is not sufficient to control the electromagnetic force. Because open loop current control is highly dependent on the coil parameters and the actual load current is usually different from the reference

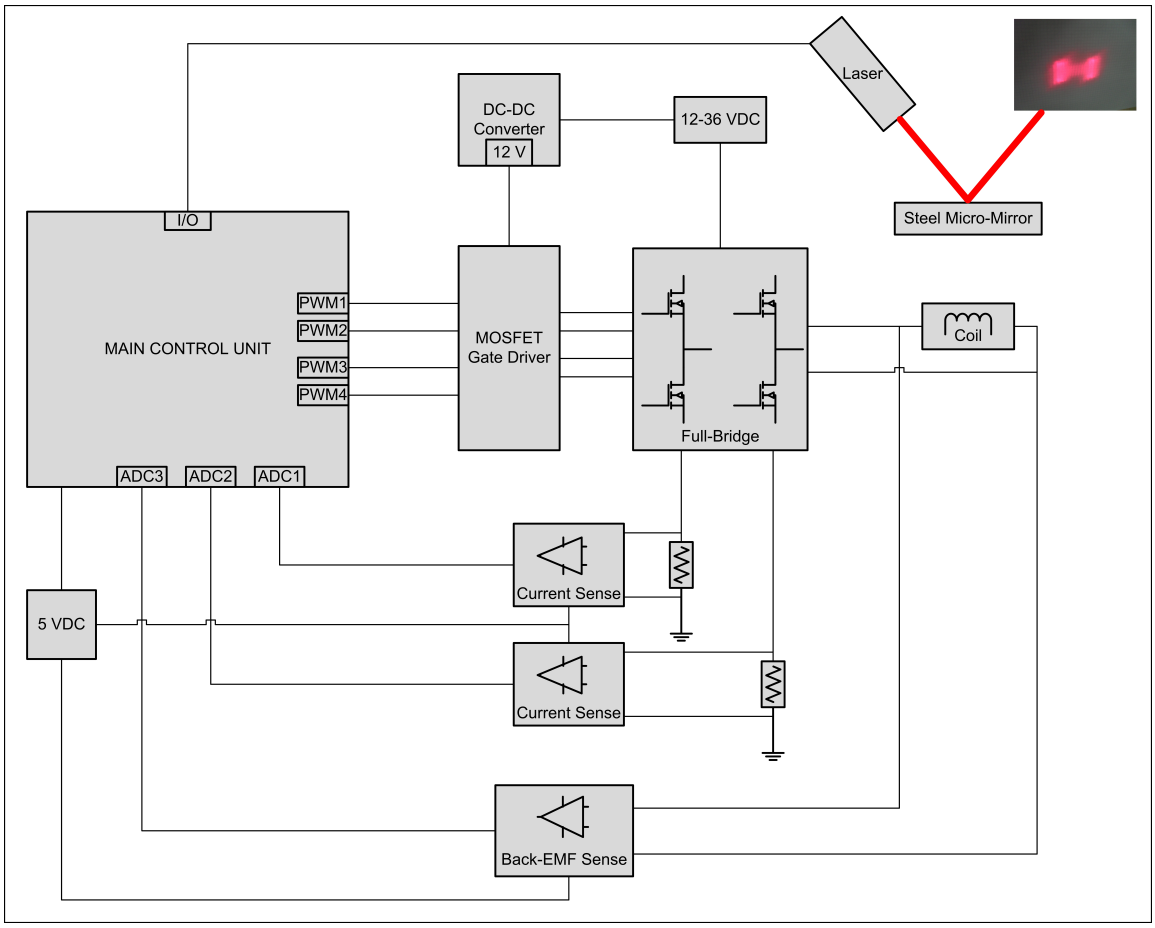

Figure 2.1. Projection display control system block diagram.

current. One could hardly manage to supply the reference current waveform to the coil with open loop current control. Closed loop current control has the advantages of accurate and instantaneous current waveform control, good dynamics, and compensation of effects of load parameter changes [14]. As a conclusion, precise direct electromagnetic force control requires closed loop current control of the actuation coil. Thus, the system is based on closed loop current control of the actuation coil.

The current control techniques developed so far could be cited as linear current control, state feedback current control, predictive current control, hysteresis current control, neural network-based current control, and Fuzzy logic-based current control [14]. The three major current control techniques which are linear, hysteresis and predictive current control [15, 16] will be explained briefly.

- *Hysteresis Current Control* :

  Hysteresis current control uses a hysteresis band around the reference current signal and forces the actual load current to remain within the boundaries of this band [17]. This current control technique is quite simple and robust but it has the disadvantage of changing switching frequency which is dependent on the load parameters [18]. Although its computation cost is very low, variable switching frequency is the major drawback which prevents this technique to be implemented in the system.
- *Predictive Current Control* :

  Predictive current control computes the voltage to be applied to the load using the load and system models in order to force the actual load current to follow the reference current [19]. This technique achieves a precise current control but it requires good knowledge of the load and system parameters and it suffers from computation burden [18]. Utilizing this technique can be considered not to be practical because changing the load or driving system means changing the system parameters in the model which could require a new load characterization and system identification.
- *Linear Current Control* :

  In linear current control, the error between the reference current and the mea-

sured current is fed to a PI controller. PI controller calculates the reference voltage which will generate the desired load current. This reference voltage is compared with a constant frequency triangle signal and switching scheme is determined [15]. Linear current control has the advantages of simplicity and fixed switching frequency. In addition to its low computation cost, it does not depend on the load and system parameters. Effects of load and system changes could be compensated easily by adjusting the PI parameters. Briefly, linear current control does not require any system identification or load characterization and it is easy to implement it with digital embedded processors.

It is decided that the most suitable current control technique for the system is linear current control technique. The choice of linear current control for the system has the following reasons:

- There is no need to load characterization and system identification. Different loads could be driven easily with a very short setup time.
- Using fixed switching frequency increases the control ability and makes timing adjustments of other system components easy.
- Generation of signals at high frequencies is easier than the other current control techniques.
- Performance of the current control can be enhanced by tuning the PI parameters.

The closed loop linear current control used in the system is depicted in Figure 2.2.

The reference signal is the sum of a high frequency sinusoidal and a low frequency saw-tooth signals. The frequencies are determined according to the micromirror characteristics. Since the waveform of the reference signal does not change during the operation it is sampled at the switching frequency rate and written to a lookup table. The actual load current is measured by the current sensing component of the system. Current sensing will be explained in detail in the following section. The PI controller has the proportional and integral parts. The error between the reference current and

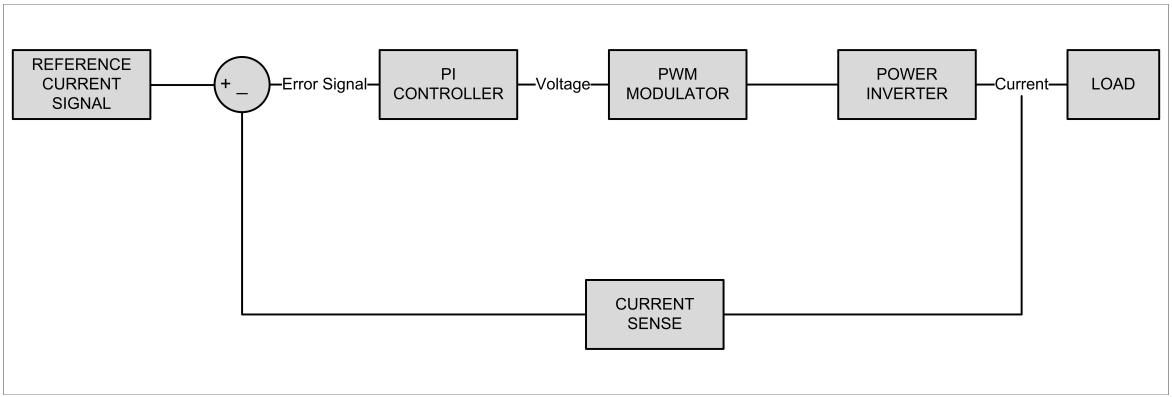

Figure 2.2. Closed loop current control block diagram.

the measured load current is processed and the reference voltage is generated by the PI controller. Since PI controller runs on a digital embedded processor, discrete time PI controller is implemented. Discrete time PI controller used in the system is formulated as below.

$$U_P(k) = K_P e(k) \tag{2.1}$$

$$U_I(k) = U_I(k-1) + K_I[e(k) + e(k-1)] \tag{2.2}$$

$$U(k) = U_I(k) + U_P(k) \tag{2.3}$$

where K_P is proportional gain, K_I is integral gain, $e(k)$ is error between the reference signal and the measured signal at sampling time k, $U(k)$ is the output of PI controller.

The reference voltage generated by the PI controller is fed to the switching modulator. Switching modulator used in the system is different from the classical triangle comparison switching modulator. Simpler switching modulator is used in the system because generating high resolution signals at frequencies around 10 kHz with

triangle comparison switching modulator is very difficult even with high performance embedded processors. Switching modulator controls the power inverter which supplies the desired current to the load. Switching modulator and power inverter will be explained in detail in Section 2.4.

2.3. Current Sensing

Current sensing is an essential part of the closed loop current control. It measures the actual load current. This measurement is the feedback of the closed loop current control. Current control performance is highly dependent on the current sensing because it monitors the actual load current which is desired to be controlled.

There are different current sensing methods used in different applications. The most commonly used current sensing methods are series sense resistor method, R_{DSON} sensing method; filter sense the inductor method, observer-based method, average current method, current transformer method and SENSEFET method [20]. Series sense resistor method uses a resistor, which is put in series with the load. It measures the voltage drop across the sense resistor and divides it by the value of the resistor to find the actual load current. Although it consumes power, its simplicity and precision make it the most widely used current sensing method. Other current sensing methods mentioned above are lossless but they have different drawbacks which make them unsuitable for the system. R_{DSON} sensing method has the disadvantage of low accuracy. Filter sense the inductor and observer-based methods require the knowledge of the load parameters. Average current method measures only the average load current, which decreases the bandwidth of the current control dramatically. Transformer current sensing method has the integration problems because of its size. SENSEFET current sensing requires special type of MOSFETs and its precision is not sufficient for the system requirements.

There are three different types of series sense resistor method, which are low-side current sensing, high-side current sensing and bi-directional current sensing [21].

In low-side current sensing shown in Figure 2.3, the sense resistor is put between the load and the ground. It is a unidirectional current sense. It has the advantages of low input common mode voltage, output voltage referenced to ground and single supply implementation. Its disadvantage is that the load is not connected to the ground directly.

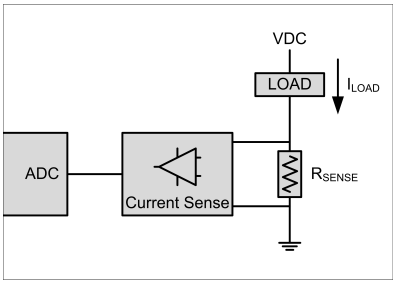

Figure 2.3. Low-side current sense block diagram.

In high-side current sensing depicted in Figure 2.4, the current on the path between the supply and the load is monitored. High-side current sensing is unidirectional. It has the advantage that the load is connected to ground but it has an important disadvantage of high input common mode voltage. Besides, the output must be level shifted down to the system operating voltage level.

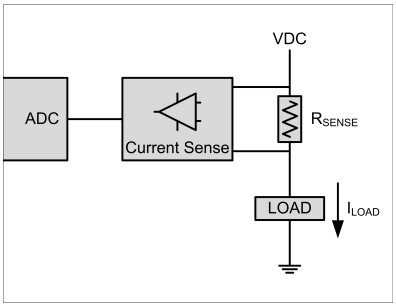

Figure 2.4. High-side current sense block diagram.

Bi-directional current sensing is demonstrated in Figure 2.5. It is a kind of high-side current sensing and it inherits the disadvantages of the high-side current sensing.

It monitors the current on the load path and has the advantage to measure the current passing through the load directly.

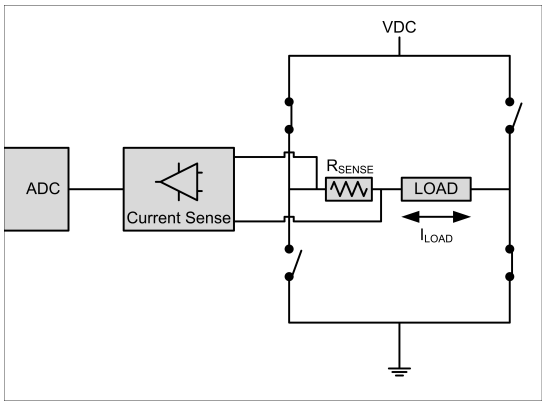

Figure 2.5. Bi-directional current sense block diagram.

Because of the implementation difficulties of high-side and bi-directional current sensing, low-side current sensing is preferred to be used in the system. The disadvantage that the load is not grounded is compensated with the MOSFET gate driver. This will be explained in detail in the power inverter section.

For efficient current sensing, sample of the current sense signal is taken in the middle of the PWM period. The current sensing circuitry implementation will be detailed in system implementation chapter.

2.4. Power Inverter

Power inverter component of the system is a single phase grid-connected full bridge inverter consisting of four n-type power MOSFETs and a MOSFET gate driver which can drive four n-type MOSFETs in full bridge configuration. Inverter operates in switch mode and is responsible to generate AC current signal from a constant voltage DC supply. The variable current of the load is controlled by chopping the fixed input voltage by varying the on and off times of the switches in the inverter. Since the linear current control technique is used, the switching frequency is fixed.

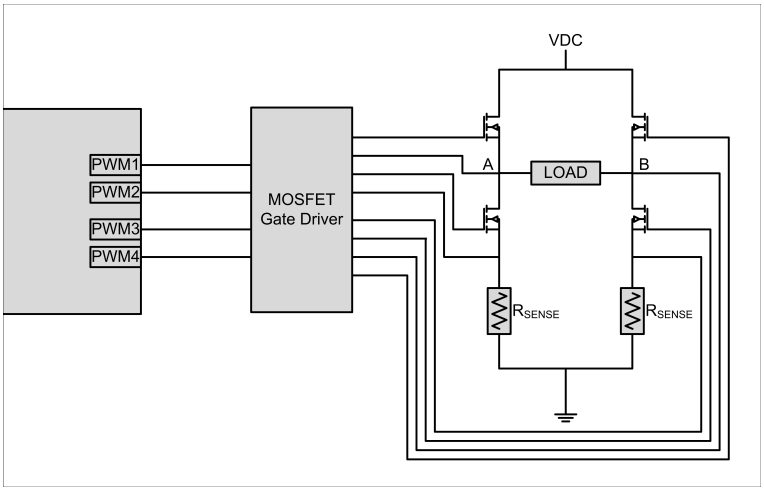

Figure 2.6. Power inverter block diagram.

The single phase grid-connected full bridge inverter in the system has the following advantages:

- There is no need to negative voltage in the system to generate the negative part of the reference current signal.
- High load currents can be achieved easily with the inverter consisting of power MOSFETs.
- Fast chopping action provides a good control on the load current. Immediate response can be given according to the current sense feedback.

Embedded processor, on which the current control algorithm runs, controls the power inverter via PWM signals. Each switching element is controlled with one PWM signal. The duty cycle of the PWM signal changes according to reference voltage output of the PI controller.

The voltage level of the PWM signals is not appropriate to drive the MOSFETs. Also, driving the high-side n-type MOSFETs requires shifting the voltage level up. Thus, a MOSFET gate driver is utilized which is capable of driving four n-type power MOSFETs. The gate driver used in the system senses the voltage at the source pin

of the low-side MOSFET and if it is necessary it shifts the voltage level of the gate of this MOSFET up. This means that the source of the low side MOSFET does not have to be connected to the ground. This compensates the disadvantage inherited from low-side current sensing.

Sinusoidal PWM technique with uni-polar switching scheme yields a good performance current control [22]. In this technique, the reference signal and the negative of the reference signal are compared with a fixed frequency triangle signal. These signals are shown in Figure 2.7a. If the reference signal is greater than the triangle signal leg A of the inverter is set active, which means that the high side MOSFET of the leg is ON and the low side MOSFET of the leg is OFF. The voltage at leg A with respect to ground is shown in Figure 2.7b. When the negative of the reference signal is greater than the triangle signal leg B of the inverter is set active. The voltage between the two nodes of the load is shown in Figure 2.7d. With this scheme, a good quality sinusoidal voltage signal with a little error, which is not shown in Figure 2.7, can be obtained.

In linear current control, sinusoidal PWM technique is used as the PWM modulator depicted in the block diagram shown in Figure 2.2. The output of the PI controller, which is the reference signal generated according to the error between desired and actual current signals, is fed to sinusoidal PWM modulator. Sinusoidal PWM modulator controls the switching of the power inverter to achieve the desired load current.

Although the sinusoidal PWM technique has a good performance, generating current signal at frequencies around 10 kHz is quite difficult with it. It requires very high speed embedded processors to compare the error signal with the triangle signal and it requires relatively complex PWM control. That is why another PWM switching scheme is used as the PWM modulator of the system.

There are five types of PWM switching schemes that can be used in a single phase grid-connected full bridge inverter other than sinusoidal PWM scheme [23]. Those are the two-quadrant PWM switching scheme, the four-quadrant simultane-

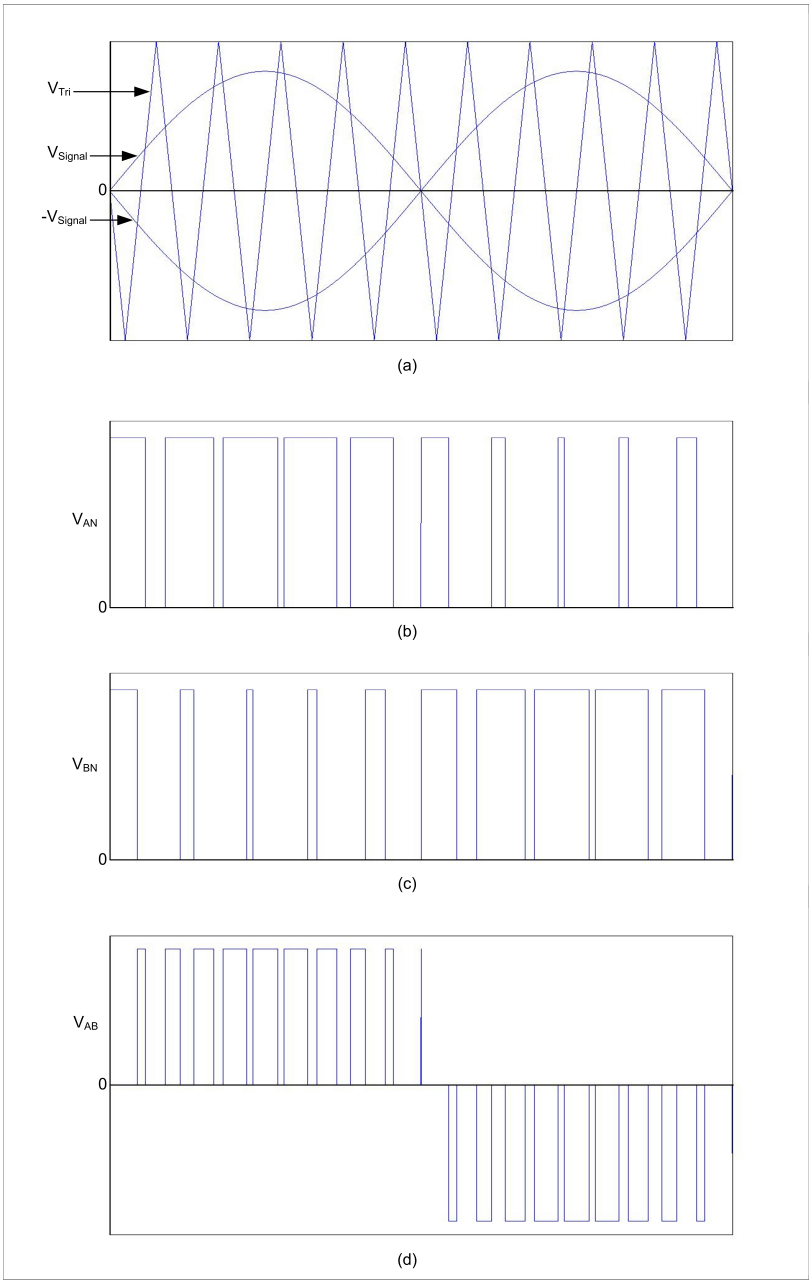

Figure 2.7. Sinusoidal PWM generation. (a) comparison of reference signal with triangle wave. (b) voltage between leg A and ground. (c) voltage between leg B and ground. (d) voltage between leg A and B.

ous PWM switching scheme, the four-quadrant simultaneous complementary PWM switching scheme, the four-quadrant non-simultaneous PWM switching scheme and the four-quadrant non-simultaneous complementary PWM switching scheme. The four-quadrant non-simultaneous complementary PWM switching scheme is superior to the other schemes and its performance is similar to that of the sinusoidal PWM scheme [23]. In addition, it reduces the noise by splitting the switching of the MOSFETs in each switching cycle and doubling the output current ripple frequency [24]. Because of these reasons, it is decided to use four-quadrant non-simultaneous complementary PWM switching scheme as the PWM modulator of the system.

Four-quadrant non-simultaneous complementary PWM switching scheme is very similar to sinusoidal PWM scheme. The difference is that the reference signal is remained constant during a period of triangle signal. This constant reference signal can be taken as the mean of the varying reference signal within a period of the triangle signal. Comparing to varying reference signal during a period of triangle signal, keeping the reference signal constant reduces the resolution of the output signal. However, it decreases the processing cost dramatically because PWM switching scheme can be determined at the beginning of the period of the triangle signal. There is no need to compare the error signal with the triangle signal multiple times within a triangle signal period.

PWM generation with four-quadrant non-simultaneous complementary PWM switching scheme is depicted in Figure 2.8. The reference signal and the negative of the reference signal are compared with the fixed frequency triangle signal. If the reference signal is greater than the triangle signal, leg A of the inverter is set active. Otherwise, it is set passive. If the negative of the reference signal is greater than the triangle signal, leg B of the inverter is set active. Otherwise, it is set passive. The state of high-side switches of leg A and leg B is the same as the state of leg A and leg B respectively. The state of low-side switches is complementary to the state of high-side switches. As shown in Figure 2.8d, switching of the MOSFETs is splitted in each switching cycle and the load current ripple frequency is doubled. This has the same effect as doubling the switching frequency.

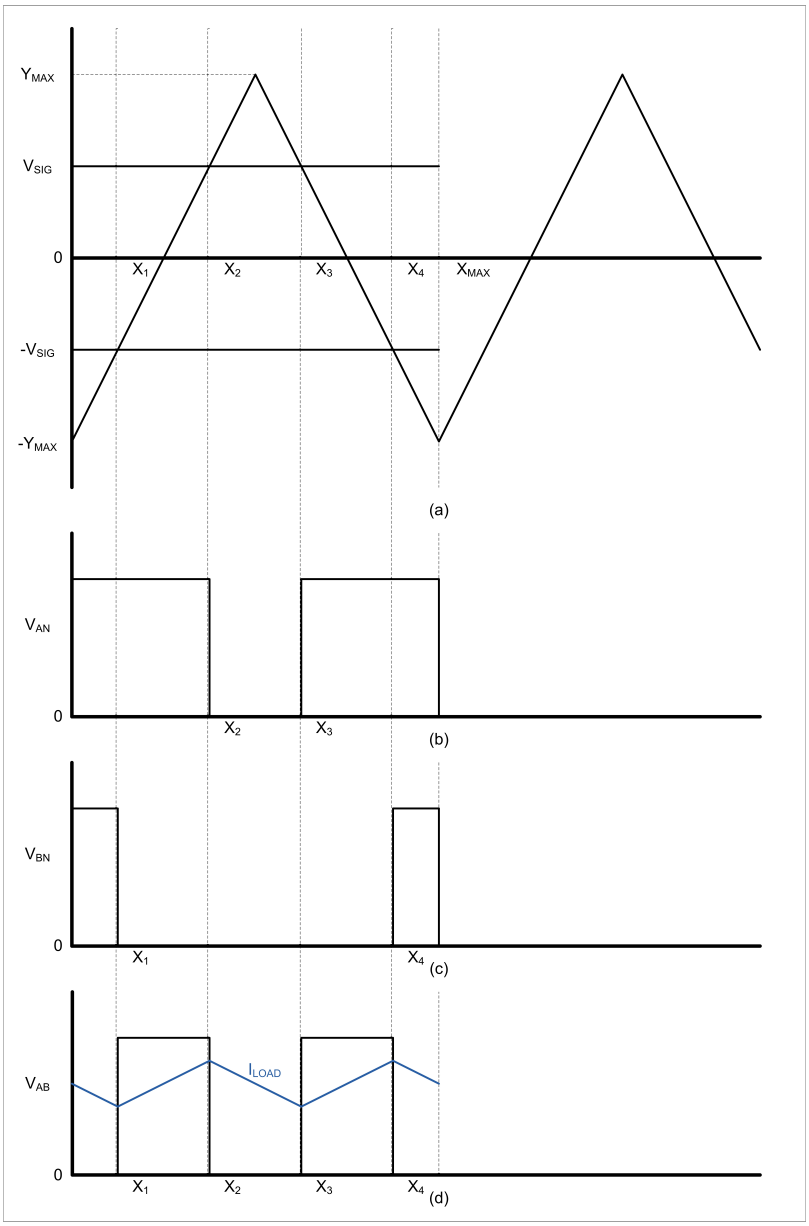

Figure 2.8. PWM modulation method used in the system. (a) comparison of reference signal with triangle wave. (b) voltage at leg A. (c) voltage at leg B. (d) load voltage and current.

The point X_1, X_2, X_3, X_4 shown in Figure 2.8a are the points where PWM signals change state. Leg B goes from high to low at X_1 and goes from low to high at X_4. Leg A goes from high to low at X_2 and goes from low to high at X_3. Using similarity theorem and using $X_{MAX} = Y_{MAX}$, X_1, X_2, X_3, X_4 are calculated as in Equation 2.4-2.7.

$$X_1 = \frac{X_{MAX} - V_{SIG}}{4} \tag{2.4}$$

$$X_4 = X_{MAX} - X_1 \tag{2.5}$$

$$X_2 = \frac{X_{MAX} + V_{SIG}}{4} \tag{2.6}$$

$$X_3 = X_{MAX} - X_2 \tag{2.7}$$

2.5. Laser Modulator

In the system, unidirectional scanning is used. A modulation lookup table, which is storing the desired image data, is created. In order to form the image according to this lookup table the knowledge of position of the light beam on the display is required. Position of the light beam is predicted using the actuating current signal. Actuating current signal is supposed to be directly related to the position of the beam. Light beam is modulated by turning on or off the laser, according to the lookup table and the position of the beam to form the desired image.

2.6. Simulation

Closed loop current control part of the system described in the previous sections is simulated using MATLAB® Simulink®. Simulink® model implementing the closed

loop current control depicted in Figure 2.2 is given in Appendix A.

Simulation model consists of the models of components of the system described in the previous sections except laser modulator. Load is modeled with a simple RL circuit. Power inverter is modeled with four n-type MOSFETs. There is no need to a MOSFET gate driver because MOSFETs are modeled as simple switches with internal ON resistance. Low-side current sensing is modeled with two resistor and two voltage measurement boxes. Simulation uses the PI controller formulated by Equations 2.1-2.3 and the PWM modulator depicted in Section 2.4. PI controller is implemented by *PI Controller* function given in Appendix A. PWM modulator is implemented by PWM, *Complementary* PWM and PWM *Modulator* functions given in Appendix A. PWM *Modulator* function implements the Equations 2.4-2.7 and PWM, *Complementary* PWM functions generate PWM signals.

In order to start the simulation, *Init* function is needed to be called. It initializes the simulation parameters and forms the lookup table of the desired current signal waveform. Simulation parameters are the real system parameters, which are measured or characterized prior to simulation. System parameters used in the simulation are given in Table 2.1.

Table 2.1. System parameters.

Parameter	**Value**	**Unit**
Fast Scan Frequency of the Mirror	11271	Hz
Slow Scan Frequency of the Mirror	281	Hz
Inductance of the Actuating Coil	0.00109	Henry
Resistance of the Actuating Coil	5.2	Ohm
ON Resistance of the MOSFETs	0.01	Ohm
Resistance of the Sense Resistors	0.2	Ohm
Current Sense Voltage Gain	16	V/V

Proportional gain of the PI controller, K_P, is set to 36/256 and the Integral gain, K_I, is set to 1/256.

Three simulations were done and the results are shown in Figure 2.9-2.16. First simulation is aimed to achieve the current signal in sinusoidal waveform at the frequency of 11271 Hz. The PWM schemes of the leg A and leg B of the inverter hence the voltages between these legs and ground are shown in Figure 2.9 and 2.10 respectively. Figure 2.11 and Figure 2.12 shows the voltages between the nodes of the sense resistors. As shown in figures, the voltage of the sense resistors are dropped to zero at some points within a current signal period. At these points, current flows through the loop consisting of two high-side MOSFETs. Although the voltage of sense resistors are discontinuous, load current is continuous at every time.

Voltage between the two nodes of the actuating coil and the load current are shown on Figure 2.13 and Figure 2.14. In order to see the PWM schemes and current sense signals clearly in relation with the load current signal, first simulation was run for only 300 us. Second simulation was run for 1 ms to see the steady state behaviour of load current. Second simulation result is shown in Figure 2.15.

Third simulation is aimed to achieve the current signal in the waveform of fast frequency sinusoidal signal plus slow frequency saw-tooth signal. The sum of these two signals actuate the mirror-scanner in 2-D, which is aimed to be achieved in real implementation. The result of the third simulation is shown in Figure 2.16.

Simulations demonstrate that the closed loop control of the actuating coil current is successfull with real system parameter values and PI controller gains. An overshoot occurs at the beginning of the current signal but the steady state beaviour of both pure sinusoidal current signal and sinusoidal current signal plus saw-tooth current signal is stable within a little error.

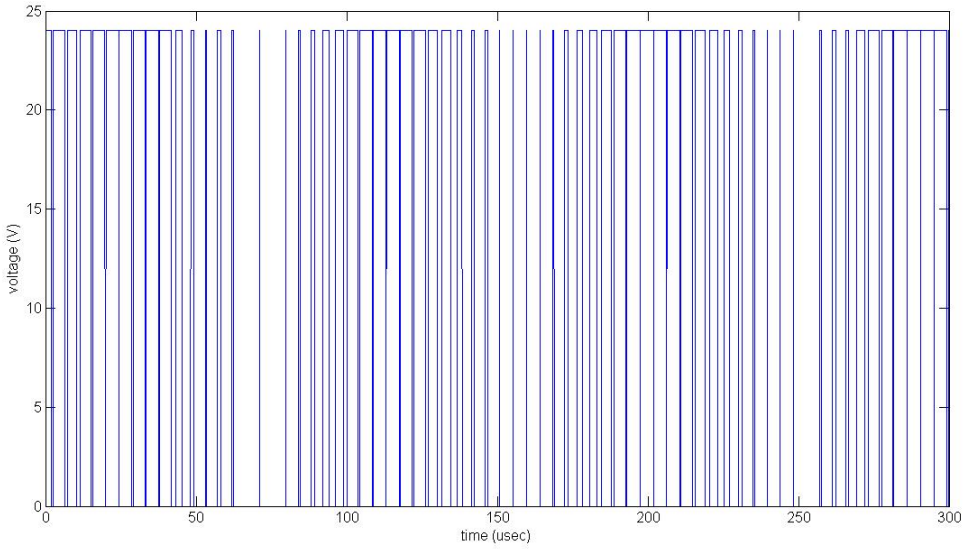

Figure 2.9. Voltage between leg A and ground.

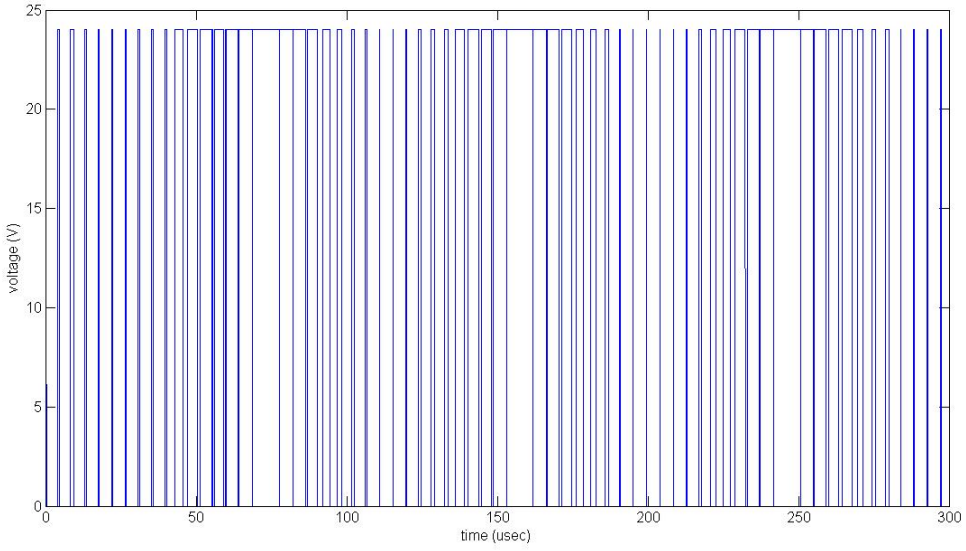

Figure 2.10. Voltage between leg B and ground.

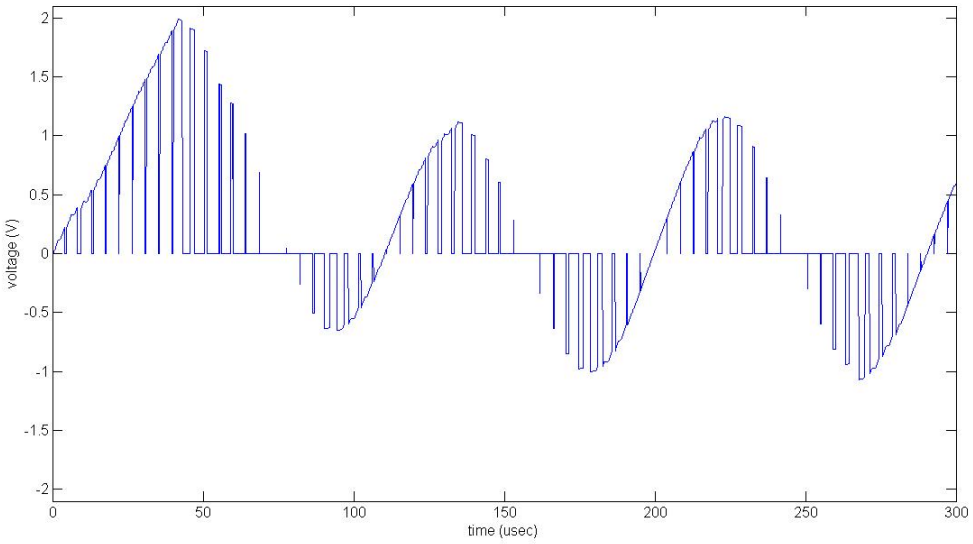

Figure 2.11. Voltage between the nodes of the sense resistor 1.

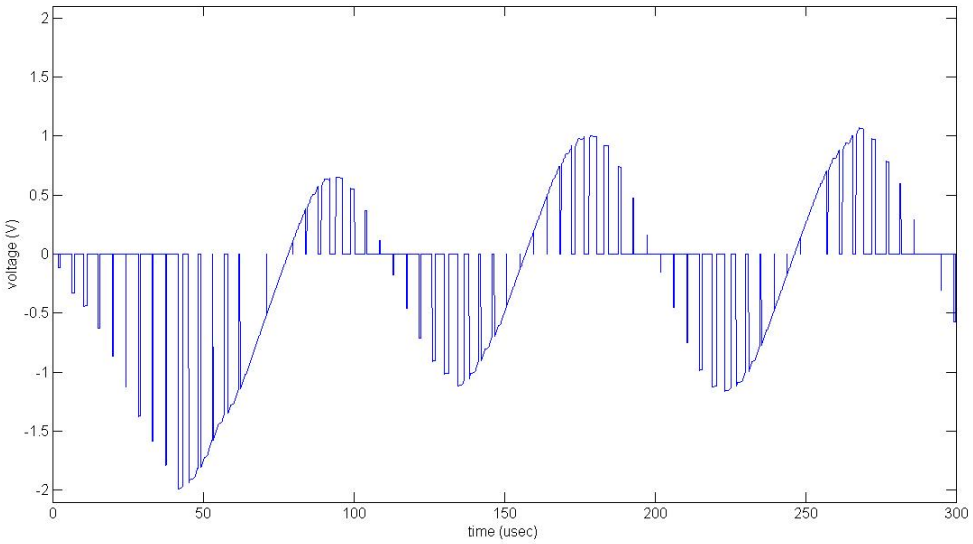

Figure 2.12. Voltage between the nodes of the sense resistor 2.

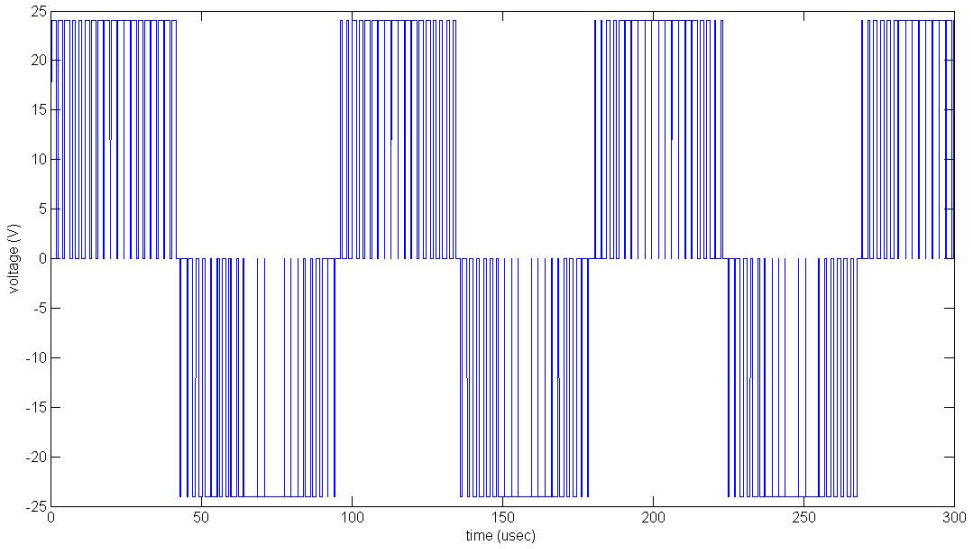

Figure 2.13. Voltage between the nodes of the load.

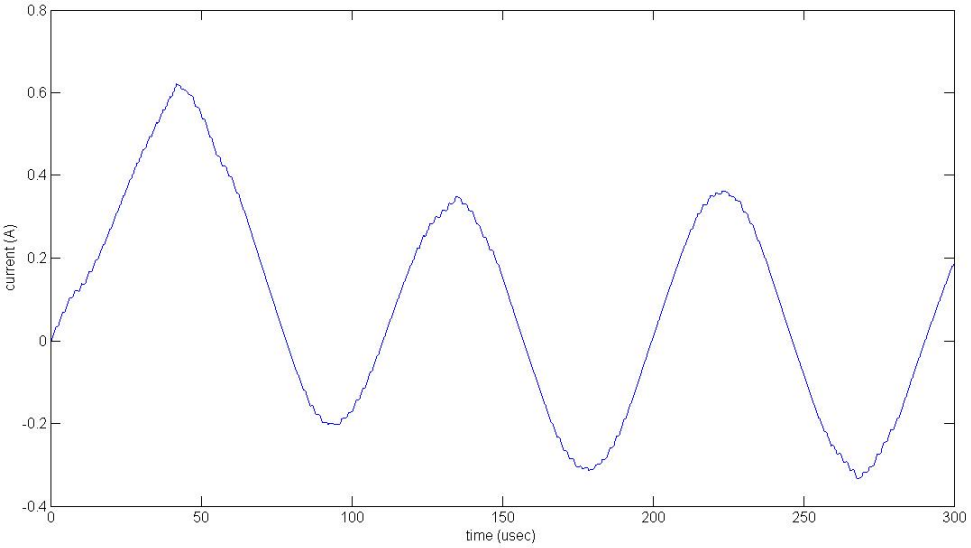

Figure 2.14. Load current in sinusoidal waveform with 300 usec simulation duration.

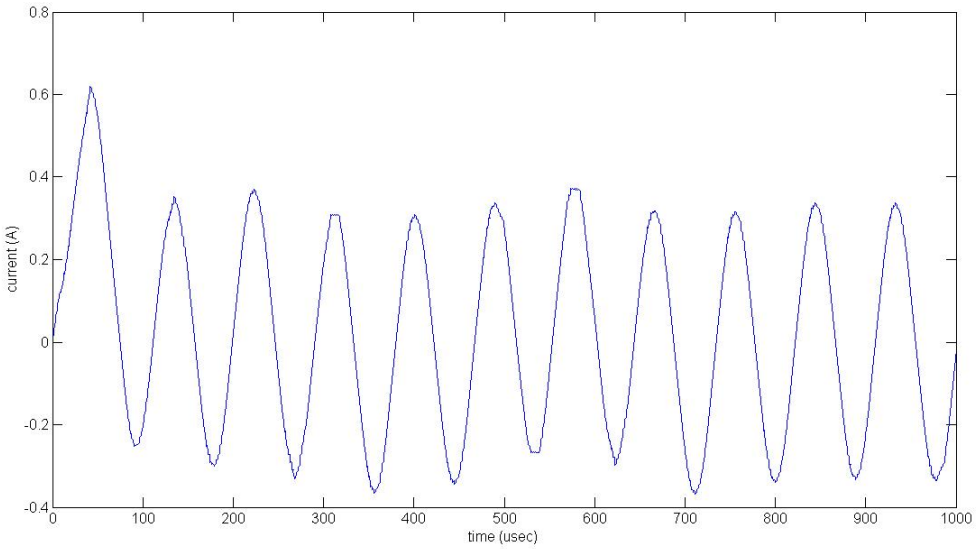

Figure 2.15. Load current in sinusoidal waveform with 1 msec simulation duration.

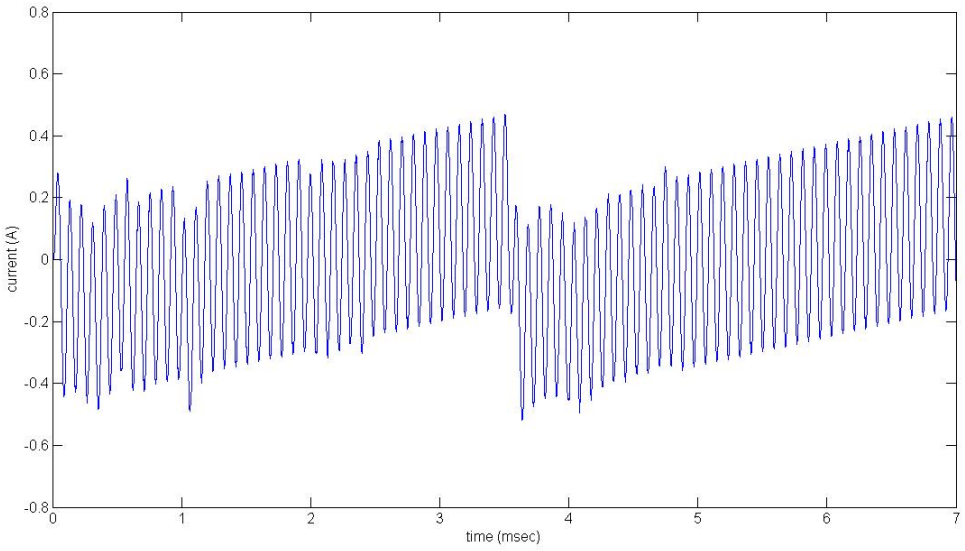

Figure 2.16. Superimposed load current consisting of high frequency sinusoidal and low frequency saw-tooth signals.

3. SYSTEM IMPLEMENTATION

System implementation is the implementation of the system described and simulated in the previous chapter. Implementation is discussed in two sections which are hardware implementation and firmware implementation.

3.1. Hardware Implementation

Hardware implementation of the system includes all the system components described in Chapter 2. Hardware of the system consists of two separate printed circuit boards including a main control unit, current sense circuitry, power inverter, laser modulator and power supplies. These two separate printed circuit boards are connected together to form the whole system.

Main control unit consists of an embedded microcontroller and the peripherals necessary for the microcontroller to work. It controls all the other system components. It is responsible to run the closed loop current control algorithm and control the modulation of the laser. Embedded microcontroller digitizes the analog output of the current sense circuitry by its ADC peripheral and controls the power inverter via PWM signals. Current sense circuitry senses the actual load current by measuring the voltage across the sense resistor and amplifying this voltage to the operation voltage level of the microcontroller. Power inverter generates desired AC current signal from a constant DC voltage. Laser modulation is done via a GPIO pin of the microcontroller connected to the modulation pin of the laser.

The system described in the previous chapter has the following requirements.

- A powerful real-time microcontroller with fast and enhanced ADC, and sophisticated PWM peripherals in order to control current signals at frequencies around 10kHz.
- Very low offset, low drift, rail to rail op-amps in current sensing circuitry because

of the small voltage range across the sense resistors.

- Fast power MOSFETs and a MOSFET gate driver with short delay time in order to control the load current with a short response time.

Special attention is needed in the PCB design of a real-time microcontroller because its operating frequency is quite high. Also, hardware of the microcontroller requires a multilayer PCB. Since design and production of a multilayer PCB is costly and time consuming, it is preferred to use an experimenter kit provided by the microcontroller manufacturer as the main control unit. Components of the system other than the main control unit is implemented with a separate two layer PCB. The design and production of this PCB is original. An advantage of using separate PCBs is to separate the high voltage power part of the hardware from the low voltage main control unit part.

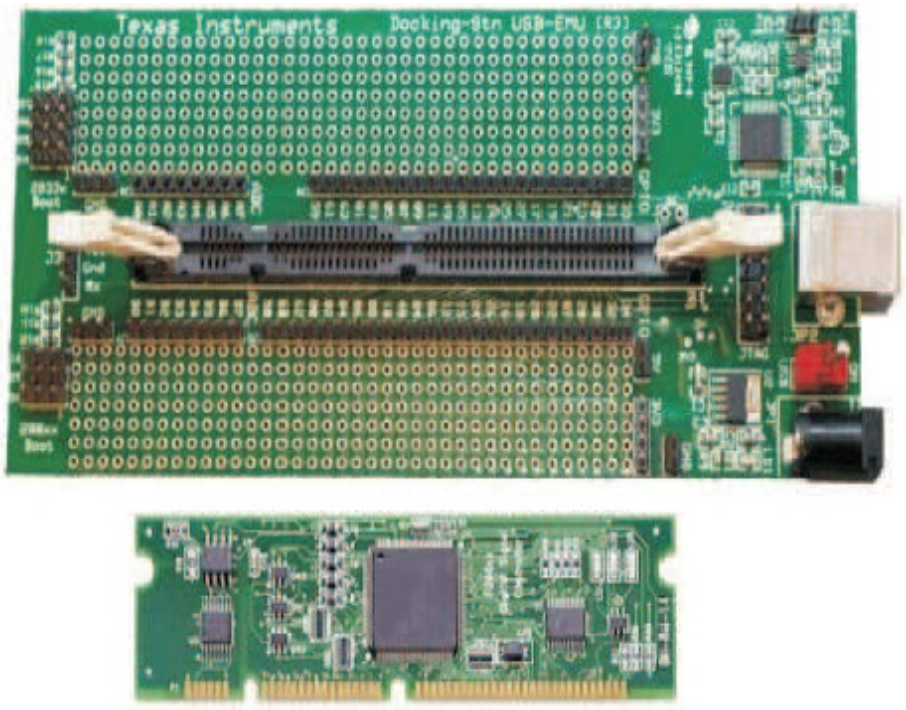

Figure 3.1. F2808 experimner kit from Texas Instruments [1].

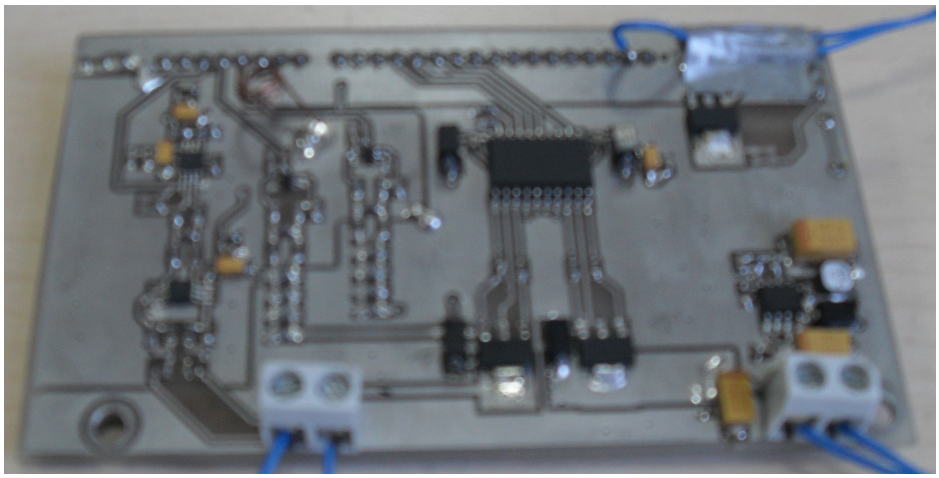

Figure 3.2. Original two layer power board.

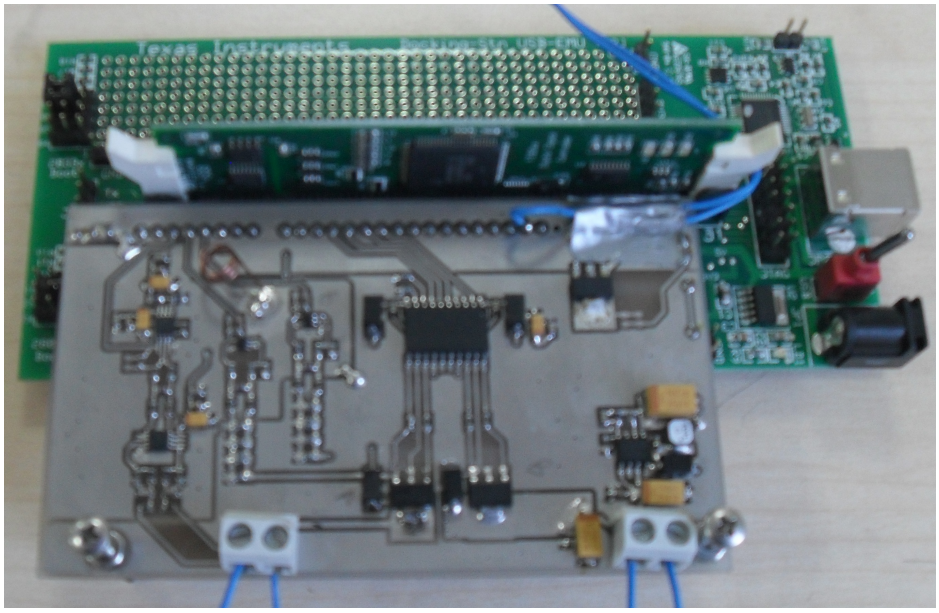

Figure 3.3. System hardware; experimenter kit and power board together.

3.1.1. Main Control Unit

Texas Instruments TMS320F2808 real-time microcontroller (abbreviated with F2808) is used as the main control unit. F2808, operating at 100 MHz, is a powerful embedded controller with sophisticated ADC and PWM peripherals. PWM peripheral has the prefix "enhanced" and abbreviated with ePWM.

Followings are some specifications of F2808 [25].

- 32-bit 100 MHz CPU
- 64K x 16 Flash, 18K x 16 SARAM Memory
- 12-bit ADC with 160 ns (6.25 MSPS) conversion rate
- Enhanced PWM with 16-bit timers.

Design and production of the PCB containing F2808 is costly and time-consuming. Thus, Texas Instruments 2808 experimenter kit with USB docking station is used as the main control unit hardware. The experimenter kit with USB docking station is shown in Figure 3.1 and pinout table of the experimenter kit is given in [26].

F2808 is very suitable to implement the closed loop current control and laser modulation described in Chapter 2. ADC module has a very fast conversion rate which makes it possible to measure the actual load current and run the current control algorithm within one PWM period. ADC can start the conversion with a trigger coming from ePWM timer and generate an interrupt when the conversion is finished. This provides accurate timing for the measurements and algorithm. ADC has two separate conversion sequences, which increases the performance of sensing current from two separate sense resistors. ePWM module is very flexible and switching modulator can be easily implemented by four ePWM outputs. ePWM timers can be synchronized altogether. Each ePWM has two different counter compare modules each of which can change the state of the PWM signal at any time within the period. Two state changes of the switching modulator are done by these counter compare modules. Details of the implementation will be explained in Section 3.2.

3.1.2. Current Sense Circuitry

Current sense circuitry is basically two difference amplifiers each of which senses the current on one leg of the inverter. The difference amplifier measures the voltage across the current sense resistor and shifts its level up to the voltage level of the F2808. Schematic of the current sense circuitry is shown in Figure B.5 in Appendix B.

Current sense circuitry has an input RC filter which eliminates the noise signals at frequencies above 10 MHz, where the switching frequency is about 200 kHz. Cut-off frequency of the input filter is

$$f_c = \frac{1}{2\pi(R_{18} + R_{25})C_1} \tag{3.1}$$

$$f_c = \frac{1}{2\pi(240 + 240)33 \times 10^{-12}}$$
$$f_c \simeq 10MHz$$

The gain of the current sense circuitry is

$$G_{cs} = \frac{R_{17}}{R_{18} + R_{21}} \tag{3.2}$$

$$G_{cs} = \frac{39k}{2.2k + 240}$$
$$G_{cs} = 15.984$$

The ADC inputs of F2808 receive voltages up to 3 Volts and the voltage amplification gain is about 16. This means that the voltage across the sense resistor must be in the range of 0-187.5 mV. In order to decrease the power losses due to sense resistor,

its value is kept small and chosen 0.2 ohm. With this configuration of the current sense circuitry, the load currents from 0 to 937.5mA can be sensed.

As the calculations exhibit, the input of the difference amplifier is in a very small voltage range, which is 0 to 187.5mV. That is why; low offset and low drift precision op-amps are required to sense currents with sense resistors. In the current sense circuitry implementation of the system, AD8627 which is a low offset, low drift and rail to rail op-amp is used.

3.1.3. Power Inverter

Power inverter component of the system is realized with four n-type power MOSFETs and a MOSFET gate driver. Power MOSFETs can handle currents up to 4 A with 0.1 ohm drain to source ON resistance. The MOSFET gate driver is HIP4081A, which can drive four n-type power MOSFETs in the full-bridge configuration. Power inverter can operate at 1 MHz switching frequency. Schematic of the power inverter is shown in Figure B.4 in Appendix B.

3.1.4. Laser Modulation

Laser modulation is done by turning on or off the laser via a GPIO pin of the microcontroller. Modulation pin of the laser is compatible with the GPIO pin of the microcontroller. Thus, these two pins are connected to each other directly.

3.1.5. Power Supplies

There are four different voltage levels in the system, which are 3.3V, 5V, 12V and the voltage varying between 12V and 36V. Main controller unit operates at 3.3V voltage level. F2808 experimenter kit provides supplies at 3.3V and 5V voltage levels. Op-amps in the current sense circuitry are supplied by the 5V provided by the experimenter kit. MOSFET gate driver drives the MOSFETs with 12V gate to source voltage and it is supplied with 12 V. This 12V supply is derived by a DC-DC con-

verter, which converts the input voltage varying between 12V and 36V to 12V. The supply voltage of the power inverter and hence the sytem can change from 12V to 36V. Schematic of the power supply is shown in Figure B.6 in Appendix B.

3.2. Firmware Implementation

Firmware, which runs on F2808, is responsible to control the actuation of the scanner and the modulation of the laser. It initializes the system parameters, generates lookup tables and controls the system components, which are power inverter, current sensing, laser modulation and PI current control. In firmware implementation, header files and example programs provided by Texas Instruments are used as reference.

Firmware runs on a digital signal controller and inherits its hardware specifications and performance. Switching frequency, which is an important issue in program timing, is determined according to CPU frequency and program loop completion rate of the digital signal controller. After implementation tests, it is decided to construct a period of high frequency signal with 20 samples and to use switching frequency according to the number of samples and the fast scan frequency.

Firmware implementation is explained in two subsections, which are Firmware Program Flow and Firmware Program Timing.

3.2.1. Firmware Program Flow

Firmware program flow is depicted in Figure 3.4. The code which implements the firmware program flow is in *main.c* file. Program starts with initializing system clock and configuring the control peripherals, which are ePWM and ADC modules. Then, it initializes firmware parameters and generates lookup tables. ADC and ePWM configurations are done according to the system timing and control requirements.

Five ePWM timers are used in the system. Four of them are used to generate PWM signals and the fifth one is used to control the system timing. Period of all of

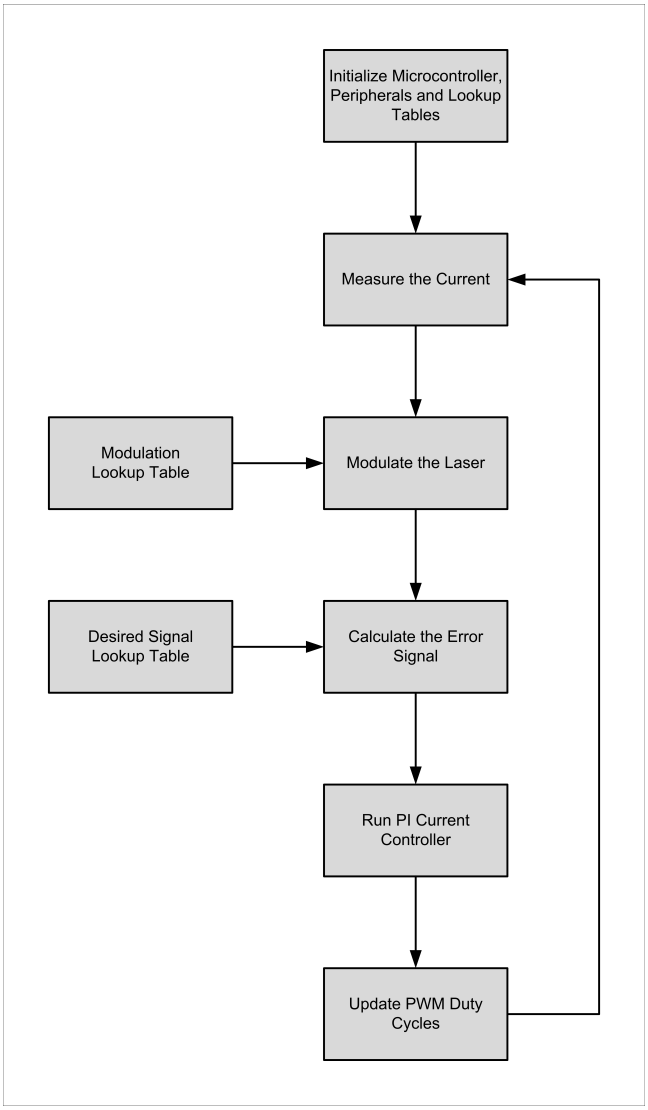

Figure 3.4. Firmware program flow block diagram.

the timers are the same and they are synchronized at the beginning of the program. It is determined so that the desired switching frequency and hence the signal at desired frequency are achieved. Four of the ePWM timers are configured so that they can control the state of the PWM signals according to the PWM modulator command. Pins associated to these four ePWM timers are also configured as PWM outputs. Fifth ePWM timer is configured to generate a trigger, which forces the ADC module to start the conversion. It does not have an output. Initialization and configuration functions of ePWM module is in ePWM.c file.

ADC starts conversion with the SOC trigger coming from the fifth ePWM timer. It has two conversion sequences each of which is configured to sense the current on one leg of the inverter. Pins associated to ADC module are configured as analog inputs. ADC generates an interrupt when the conversion is finished and result is written to the associated register. Initialization and configuration functions of ADC module is in ADC.c file.

The desired signal lookup table generated by simulations is used in the implementation. It is hard-coded and kept in an array. Modulation lookup table is generated manually and is also hard-coded and kept in an array.

After initialization part is completed, program runs a loop, which is based on ADC interrupt routine. ADC starts conversion with the SOC trigger and generates an interrupt when the conversion data is ready to be used. The interrupt routine starts when the digital conversion data is ready. It includes the rest of the parts of program flow, which are “Modulate the Laser”, “Calculate the Error Signal”, “Run PI Current Controller”, “Update PWM Duty Cycles”. Pseudo code of the interrupt routine is given below. Code of the interrupt routine is given in Appendix B.

Fast scan frequency of the micromirror used in the work is nearly 40 times of its slow scan frequency. In order to achieve synchronization, fast scan frequency is taken what it is and slow scan frequency is taken one forty of fast scan frequency. The signal at fast scan frequency is constructed with 20 samples. This means that the

```
define MaxSinusoidalIndex as 20;
define MaxSawtoothIndex as 400;
define MinSawtoothIndex as -400;
define MaxModulationIndex as 800;
Modulate the laser;
if Reference signal is negative  then
   Use ADC sequence 1 and calculate the error;
else
   Use ADC sequence 2 and calculate the error;
end if
Run PI current controller using Equations 2.1-2.3;
if Control signal is exceeds limits then
   Equate it to limit;
end if
Run PWM modulator using Equations 2.4-2.7;
Update PWM duty cycles;
Increase the sinusoidal signal lookup table index;
if Index is equal to MaxSinusoidalIndex then
   Equate index to zero;
end if
Increase the modulation lookup table index;
if Index is equal to MaxModulationIndex then
   Equate index to zero;
end if
Increase the saw-tooth signal index;
if Index is equal to MaxSawtoothIndex then
   Equate index to MinSawtoothIndex;
end if
```

Figure 3.5. First part of the interrupt routine pseudocode.

Compute the new reference signal using
$SinusoidalSignalLuT[SinusoidalIndex] + 2SawtoothIndex$;
if New reference signal is negative **then**
  Prepare ADC sequence 1 to sense the current on leg B;
else
  Prepare ADC sequence 2 to sense the current on leg A;
end if
Prepare for the new interrupt;

Figure 3.6. Second part of the interrupt routine pseudocode.

signal at slow scan frequency is constructed with 800 samples. Modulation is done in every sample. By interpolation, modulation can be done several times in every sample. This will increase the resolution in fast scan axis. Generating a period of slow scan frequency signal yields one frame of prjection display. There are 800 points in one frame of display. Thus, there are 800 elements in modulation lookup table.

Sawtooth signal which yields slow scan of the micromirror, is constructed using a variable which is monothonically increasing from -400 to 400. When this variable reaches 400, period of the slow scan signal is completed and the variable is set to -400. Sinusoidal signal at fast scan frequency is kept in a lookup table with 20 samples. Another variable which ranges from 0 to 20 is used for indexing the lookup table. When this variable reaches 20, period of the fast scan signal is completed and the variable is set to 0. The two variables used for generating fast and slow scan signals, are synchronized so that 40 periods of fast scan signal is equal to one period of slow scan signal. The superimposed signal which has high frequency sinusoidal signal and low frequency saw-tooth signal components, constructed by adding the product of a constant and the variable which ranges from -400 to 400, to the value of the element of the lookup table indexed by the variable which ranges from 0 to 20.

3.2.2. Firmware Program Timing

Firmware program timing is depicted in Figure 3.7. ePWM5 timer is used to manage the firmware timing. ePWM5 timer counts up to a specified value and than resets to zero. The period of ePWM5 timer which is same as those of the other ePWM timers, is determined according to the switching frequency. Switching frequency is calculated as below. f_s is the switching frequency, n is the number of samples in one period of fast scan signal and f_f is the fast scan frequency.

$$f_s = nf_f$$
$$f_s = 20 \times 11271 = 225420$$

The maximum value to which ePWM5 timer counts up is calculated by dividing the ePWM timer clock frequency by the switching frequency. ePWM timer uses system clock which is 100 MHz. However, experiments done to measure the system clock shows that it is different from 100 MHz and it is approximately 100.54 MHz. This can be expected because the frequency of the crystal used for clock generation has a tolerance. The maximum value to which ePWM5 counts up is calculated as below. One count of ePWM5 timer is 9.9439 nsec.

$$c_{max} = \frac{f_{op}}{f_s}$$
$$c_{max} = \frac{100537320}{225420} = 446$$

Current sensing is done in the middle of the PWM period. In order to take a sample in the middle of the PWM period, SOC trigger is generated 28 clock before the half of the PWM period. After taking the sample, ADC finishes the conversion and generates an interrupt 32 clock after the sampling. Interrupt routine starts with this interrupt. In the routine, current control algorithm runs and PWM duty cycles are updated before the end of the PWM period. So, the new PWM period starts with the

updated PWM duty cycles. Rest of the interrupt routine exceeds to the new PWM period but it is ensured that it finishes before the new SOC trigger.

The system is adjusted to generate 11271 fast scan frequency. However, higher fast scan frequencies can be achieved by increasing the switching frequency and decreasing the number of samples in one period. System is capable to generate 16000 fast scan frequency.

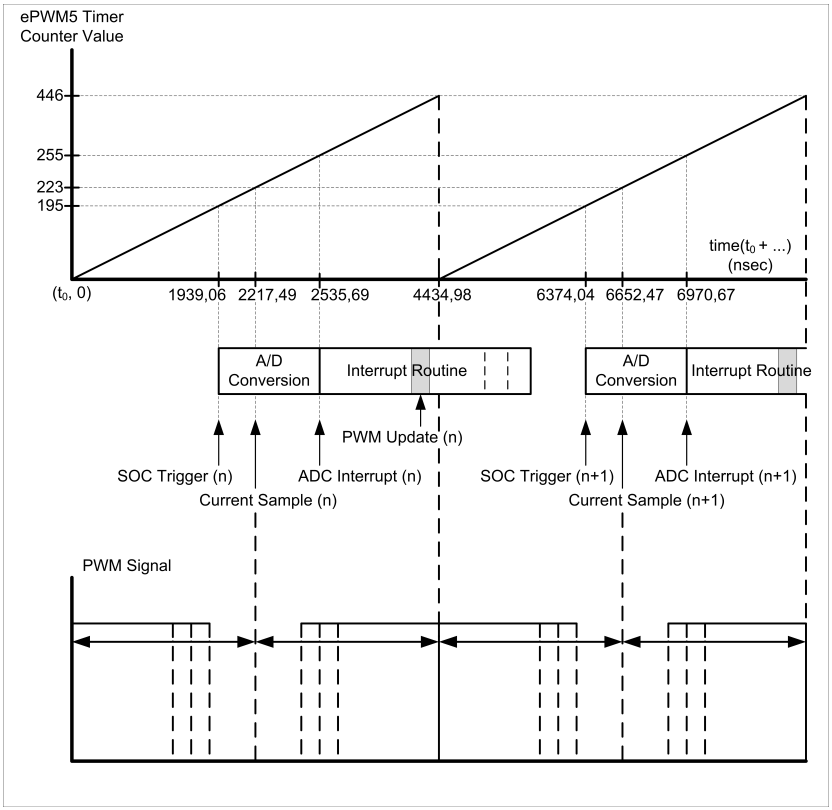

Figure 3.7. Firmware timing diagram.

4. EXPERIMENTS AND RESULTS

Experiments were done using the realized projection display control system and the steel micromirror. Micromirror has the fast scan frequency of 11271 Hz and slow scan frequency of 285 Hz. In the experiments an electro-coil and a permanent magnet is used to generate magnetic fields. The micromirror and the electro-coil mounted behind the micromirror are shown in Figure 4.1. The system component parameters are the same as given in Table 2.1. The experimental setup is shown in Figure 4.2.

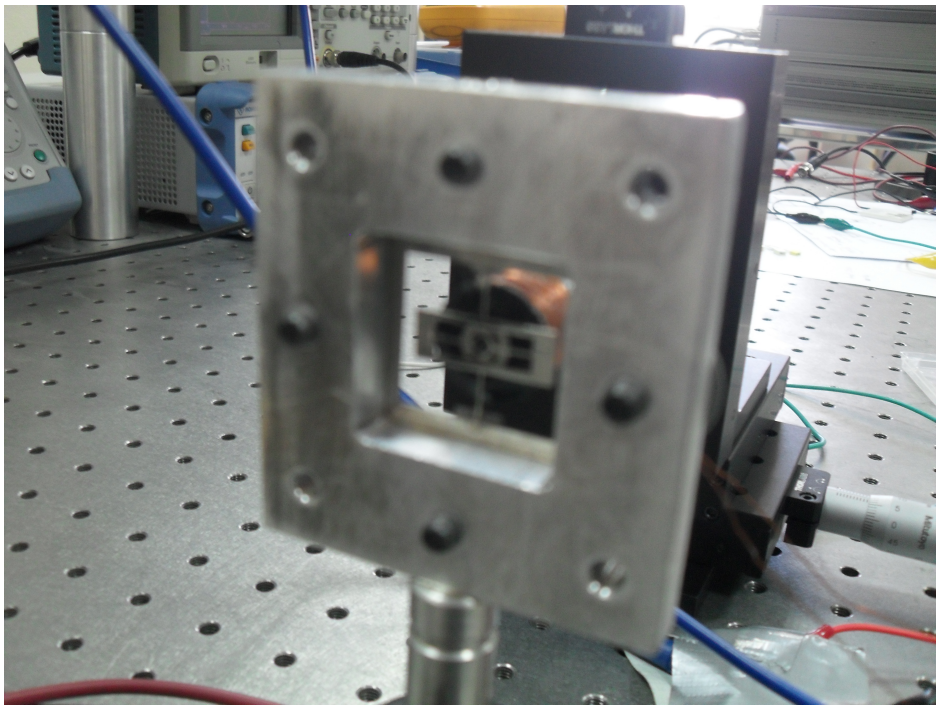

Figure 4.1. Steel micromirror scanner attached on a holder.

Before projection display experiments, actuating coil current signal waveforms are examined. The voltage signals on the current sense resistors are shown in Figure 4.3. Yellow signal shown in the figure is the voltage of the current sense resistor 1 and it is measured by channel 1 of the oscilloscope. Green signal shown in the figure is the voltage of the current sense resistor 2 and it is measured by channel 2 of the oscilloscope. Purple signal is a math function which subtracts signal 2 from signal 1.

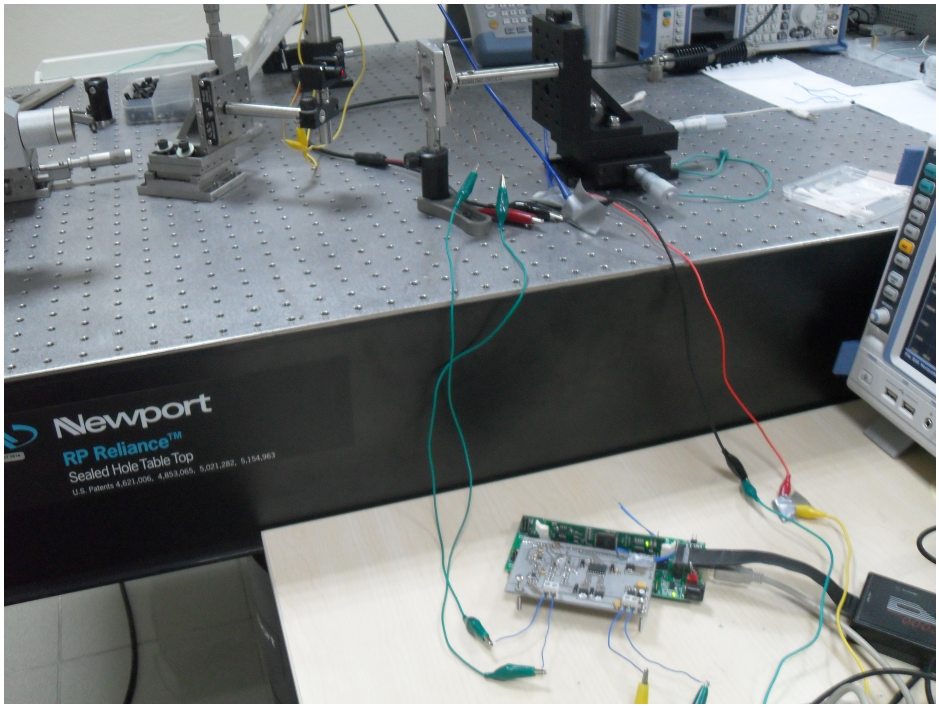

Figure 4.2. Experimental setup.

Current sense signals are consistent with simulation results shown in Figure 2.11 and 2.12. Signals drops to zero at some points in one period. This is becuse four-quadrant non-simultaneous complementary PWM switching is used. At those points current is passing through the loop consisting of two high side MOSFETs.

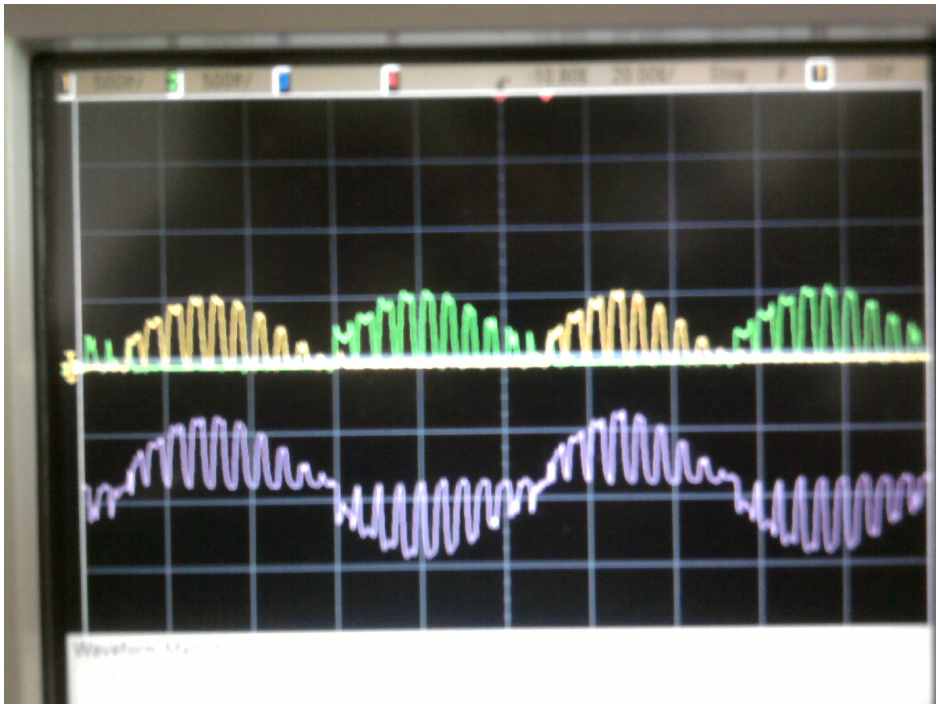

Figure 4.3. Current sense waveforms.

Before applying superimposed current signal to the actuating coil, sinusoidal current signal at fast scan frequency is applied. It is shown in Figure 4.4. The current signal obtained is the desired current signal and is consistent with simulation results shown in Figure 2.15.

Superimposed current signal which yields 2D scan is examined before forming the projection display. It is shown in Figure 4.5. It has two components, which are slow scan saw-tooth current signal and fast scan sinusoidal current signal.

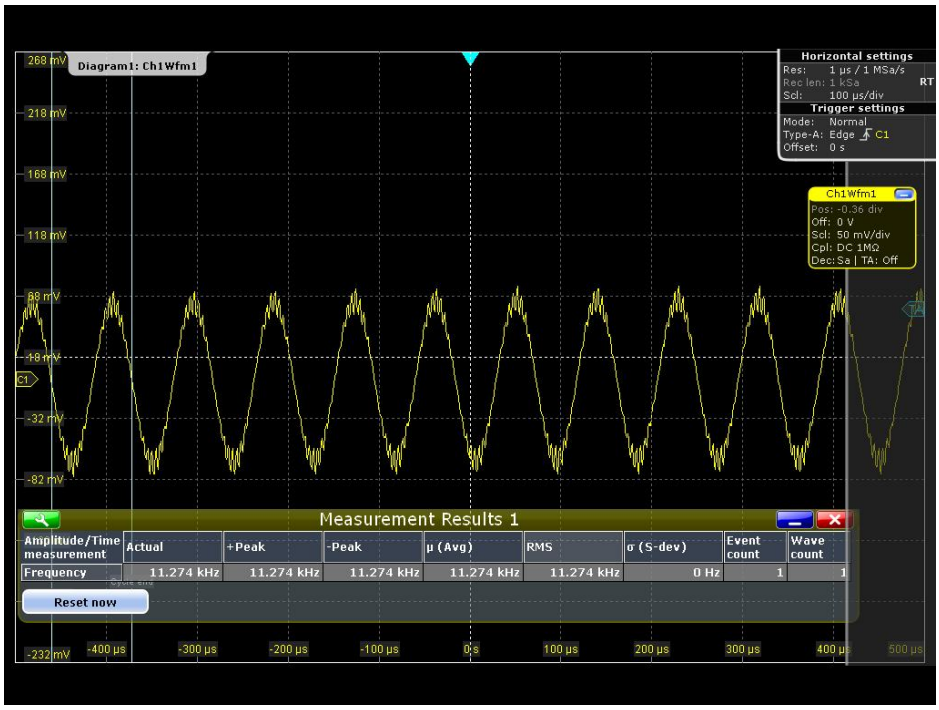

Figure 4.4. Fast scan current signal in sinusoidal waveform.

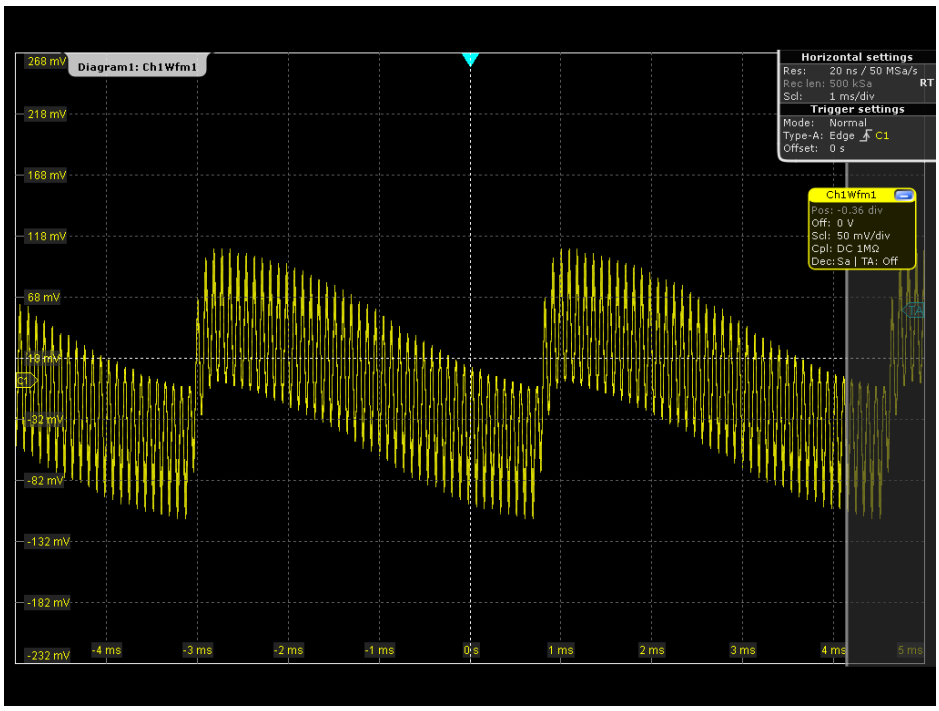

Figure 4.5. Superimposed current signal consisting of high frequency sinusoidal and low frequency saw-tooth signals.

Two different 2D raster scan which are obtained by applying the superimposed current signal, are shown in Figure 4.6 and 4.7. Their width and height are different. As it may be seen from the figures when the height of the scan increases width of the scan decreases. This is related to the position of the actuating coil. As the actuating coil is coming close to the center of the scanner from the sides height of the raster scan is getting larger.

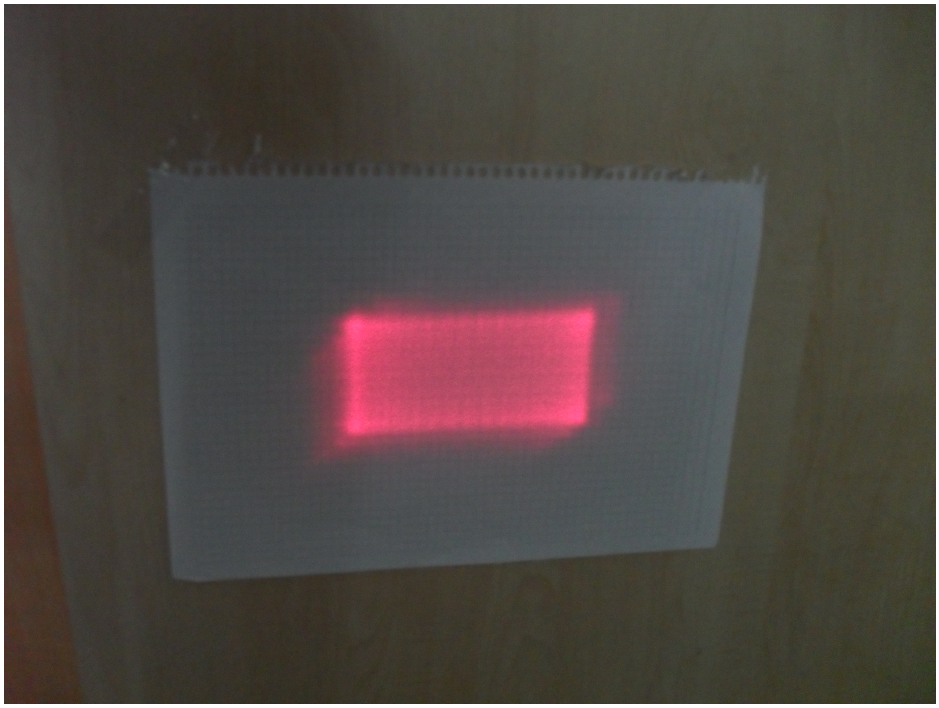

Figure 4.6. 2D raster scan with height of 6 cm and width of 12.5 cm.

The raster scan shown in Figure 4.7 has the height of 7 cm and width of 10 cm. The distance between the display and the micromirror is 120 cm. The TOSA of the slow scan is 2.39° and the TOSA of the fast scan is 3.35°. In image formation, this 2D raster scan is used.

Two images achieved using bidirectional scanning are shown in Figure 4.8 and 4.9. It is written EFE on the displays. E and F characters are chosen to be projected because it is relatively easy to modulate them in the scan.

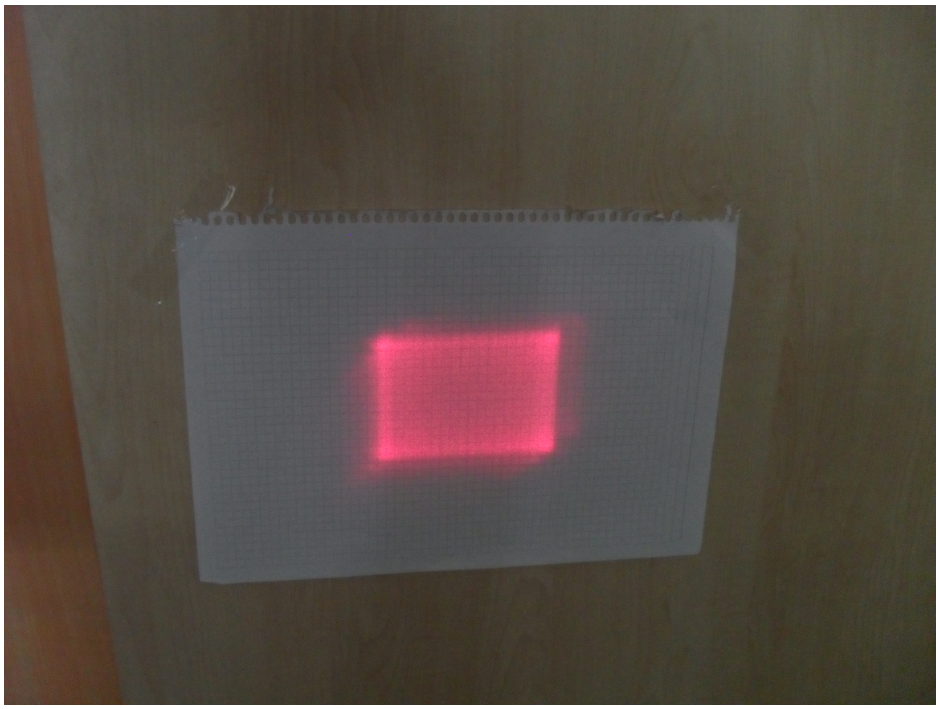

Figure 4.7. 2D raster scan with height of 7 cm and width of 10 cm.

Figure 4.8. First image on the projection display.

Figure 4.9. Second image on the projection display.

5. CONCLUSION

A projection control system, which is capable to control the actuation of the micromirror whose specifications meet the VGA display format requirements, is designed, simulated and realized. System uses closed loop linear current control to control the actuation. Simulation of the closed loop current control is done for signals in different waveforms and at different frequencies. Results of the simulation show that the designed system fulfills the VGA projection display requirements.

Realization of the designed and simulated system is done with a digital signal controller. Experiments were done with the realized system and a micromirror. The actuating coil current signals obtained in the experiments are the desired signals and consistent with the simulation results. The micromirror used in the experiments is made up with steel. It is fabricated with EDM and electroplated with Nickel. The fast scan frequency of the micromirror is 11271 Hz and the slow scan frequency is 285 Hz. Using unidirectional scanning, images in 20x40 pixels in resolution are achieved. The height of the achieved display is 7 cm and the width is 10 cm. The distance between the micromirror and the projection display is 120 cm. The TOSA of the slow scan is 2.39° and the TOSA of the fast scan is 3.35°. These parameters yield 2.51 deg.mm product θD.

The specifications of the projection display do not meet the VGA display format requirements. However, they are consistent with the micromirror specifications. Higher quality projection displays could be achieved with micromirrors which have better characteristics.

In future, projection display control system can be enhanced by developing the reflected beam spatial position sensing. This will improve the modulation and better images will be obtained. Spatial position of the reflected beam can be determined by sensing the micromirror position while scanning. Different types of position sensors can be used to predict the position of the micromirror. However, back-EMF measurement

of the actuating electro-coil may be a good technique to sense the position of the micromirror without using extra components.

APPENDIX A: SIMULATION

```
clear all
clc
global CPUFrequency;
global PWMFrequency;
global SigFrequency;
global PWMPeriod;
global PWMMaxTick;
global StepSize;
global SigMaxTick;
global PIControllerOutSig;
global IntegralIn;
global IntegralInPrev;
global ProportionalIn;
global PIError;
global PIErrorPrev;
global PGain;
global IGain; \\global CSAtoDig;
CPUFrequency = 111808320
PWMFrequency = 225420
SigFrequency = 11271
SigConstant  = 40
```

Figure A.1. First part of the initialization function.

```
RampSigFreq  = SigFrequency/SigConstant
PWMPeriod    = 1/PWMFrequency
PWMMaxTick   = CPUFrequency / PWMFrequency
StepSize     = PWMPeriod / PWMMaxTick
SigMaxTick   = (PWMFrequency/SigFrequency)*SigConstant
PIControllerOutSig = 0;
IntegralIn = 0;
IntegralInPrev = 0;
ProportionalIn = 0;
PIError = 0;
PIErrorPrev = 0;
PGain = 0;
IGain = 0;
CSAtoDig = 4096/3; %3 volt to 12 bit
funcstr= '3000*sin(2*pi*11271*x)+400000*x-709.8';
xmin=0;
xmax=(1/SigFrequency)*SigConstant;
xdt=ufix(16);
xscale=xmax/SigMaxTick;
ydt=sfix(16);
yscale=2^-16;
rndmeth='Floor';
errmax=2^-10;
spacing='pow2';
[xdata, ydata, errWorst]=fixpt_look1_func_approx(funcstr,xmin,xmax,
                                                 xdt,xscale,ydt,
                                                 yscale,rndmeth,errmax,
                                                 [],spacing);
```

Figure A.2. Second part of the initialization function.

```
function out = PWM(in)
CMPA        = in(1); %Compare A
CMPB        = in(2); %Compare B
Clock       = in(3); %Clock
StepSize    = in(4); %Simulation Step Size
PWMMaxTick  = in(5); %PWM period
PWMClock    = Clock/StepSize;
PWMClockMod = mod(PWMClock, PWMMaxTick); % Modulo Clock [0 - PWMMaxTick]
if(PWMClockMod==0)
    out = 1;
else if(PWMClockMod<CMPA)
        out = 1;
    else if(PWMClockMod == CMPA)
            out = 0;
        else if(PWMClockMod < CMPB)
                out = 0;
            else if(PWMClockMod == CMPB)
                    out = 1;
                else if(PWMClockMod>CMPB)
                        out = 1;
                    end
                end
            end
        end
    end
end
```

Figure A.3. PWM generator function.

```
function out = PWMComp(in)
CMPA        = in(1); %Compare A
CMPB        = in(2); %Compare B
Clock       = in(3); %Clock
StepSize    = in(4); %Simulation Step Size
PWMMaxTick  = in(5); %PWM period
PWMClock    = Clock/StepSize;
PWMClockMod = mod(PWMClock, PWMMaxTick); % Modulo Clock [0 - PWMMaxTick]
if(PWMClockMod==0)
    out = 0;
else if(PWMClockMod<CMPA)
        out = 0;
    else if(PWMClockMod == CMPA)
            out = 1;
        else if(PWMClockMod < CMPB)
                out = 1;
            else if(PWMClockMod == CMPB)
                    out = 0;
                else if(PWMClockMod>CMPB)
                        out = 0;
                    end
                end
            end
        end
    end
end
```

Figure A.4. Complementary PWM generator function.

```
function out = Controller(in)
Signal     = in(1);
PWMMaxTick = in(2);
if(Signal>PWMMaxTick)
    Signal=PWMMaxTick
end
if(Signal<-PWMMaxTick)
    Signal = -PWMMaxTick
end
ACMPA = round((PWMMaxTick + Signal)/4);
ACMPB = PWMMaxTick - ACMPA;
BCMPA = round((PWMMaxTick - Signal)/4);
BCMPB = PWMMaxTick - BCMPA;
out(1) = BCMPA;
out(2) = BCMPB;
out(3) = ACMPA;
out(4) = ACMPB;
```

Figure A.5. PWM modulator function.

```
function out = PIController(in)
global StepSize;    %Simulation Step Size
global PWMMaxTick;  %PWM period
global SigMaxTick;
global LookupTable;
global PIControllerOutSig;
global IntegralIn;
global IntegralInPrev;
global ProportionalIn;
global PIError;
global PIErrorPrev;
global PGain;
global IGain;
global CSAtoDig;
PGain = 36/256;
IGain = 1/256;
CurrentA   = in(1); %Compare A
CurrentB   = in(2); %Compare B
Clock      = in(3); %Clock
```

Figure A.6. First part of the PI controller function.

```
PWMClock    = Clock/StepSize;
PWMClockMod = mod(PWMClock, PWMMaxTick); % Modulo Clock [0 - PWMMaxTick]
SigClock    = floor(PWMClock/PWMMaxTick);
SigClockMod = mod(SigClock, SigMaxTick)+1;
if(PWMClockMod==(PWMMaxTick/2-1))
    CurrentA = CurrentA*CSAtoDig;
    CurrentB = CurrentB*CSAtoDig;
    if(CurrentA>=CurrentB)
        PIError = LookupTable(SigClockMod) - CurrentA;
    else
        PIError = LookupTable(SigClockMod) + CurrentB;
    end
    ProportionalIn     = PIError*PGain;
    IntegralIn         = IntegralInPrev + IGain*(PIError + PIErrorPrev);
    PIControllerOutSig = round(ProportionalIn + IntegralIn);
    IntegralInPrev     = IntegralIn;
    PIErrorPrev        = PIError;
end
out = PIControllerOutSig
```

Figure A.7. Second part of the PI controller function.

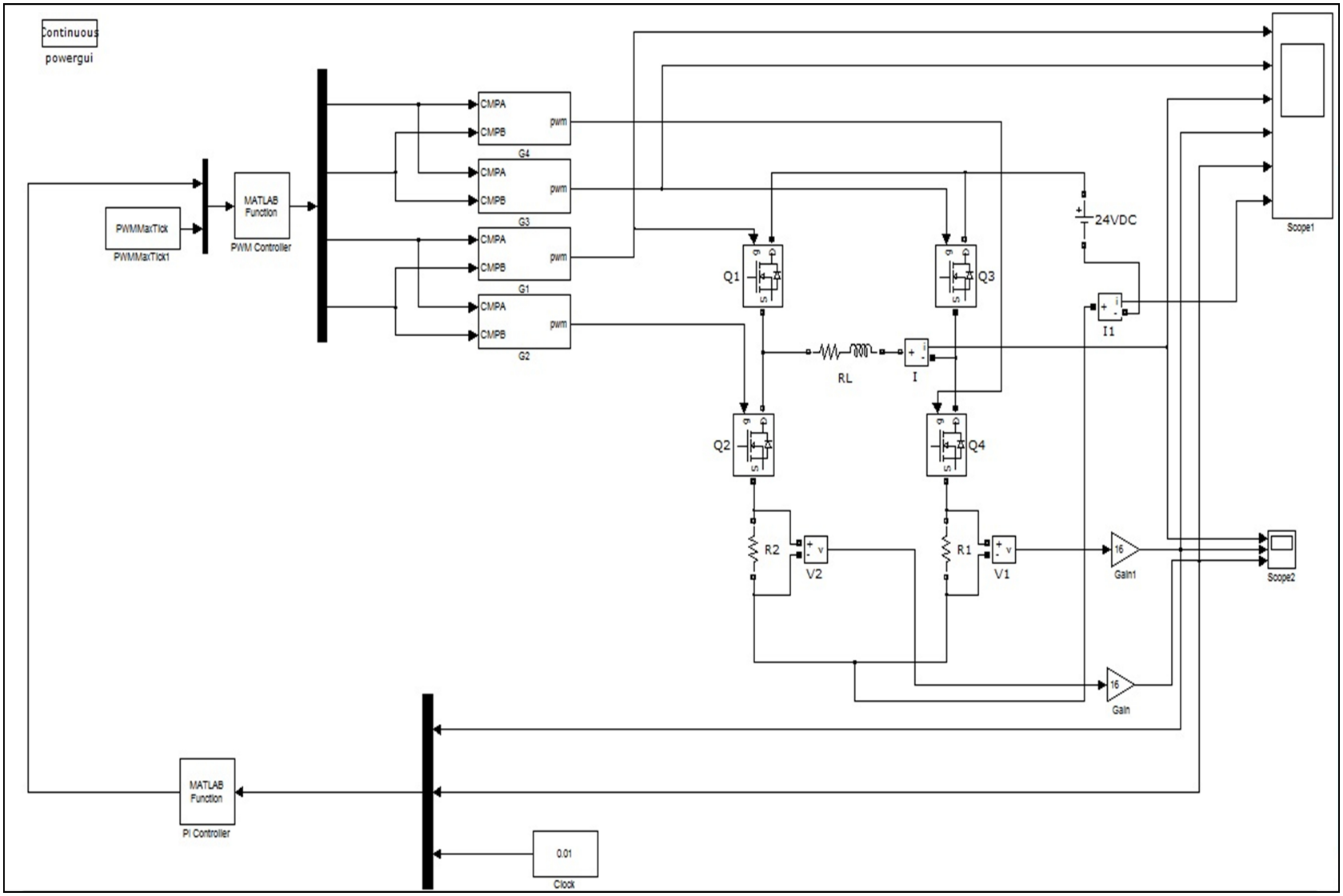

Figure A.8. Simulation model.

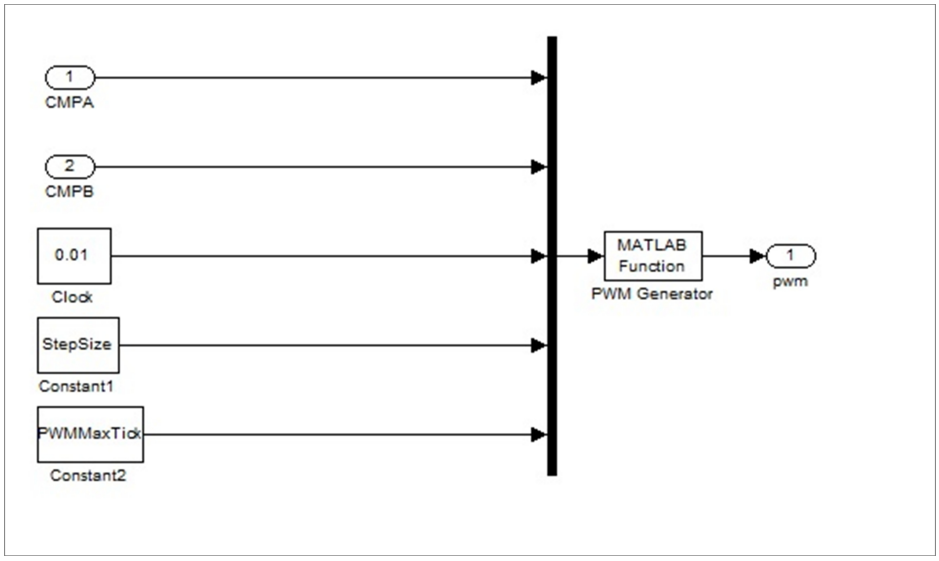

Figure A.9. PWM generator model.

APPENDIX B: IMPLEMENTATION

```
interrupt void  adc_isr(void){
  PieCtrlRegs.PIEIER1.bit.INTx6 = 0;
  GpioDataRegs.GPADAT.bit.GPIO26 = ModText[TextIndex];
  if(SigValueRef<0){
    PIError = SigValueRef + AdcMirror.ADCRESULT0;
  }else{
    PIError = SigValueRef - AdcMirror.ADCRESULT8;
  }
  IntegralIn = IntegralInPrev + IGain*(PIError + PIErrorPrev);
  PISigValue = IntegralIn + PGain*PIError;
  if(PISigValue > SigValueMaxAF){
    PISigValue = SigValueMaxAF;
  }
  if(PISigValue < -SigValueMaxAF){
    PISigValue = -SigValueMaxAF;
  }
  ASideCMPA = (PWMCountMaxAF + PISigValue)/4096;  // = x2 - 4*8*128
  ASideCMPB = PWMCountMax   - ASideCMPA;          // = x3
  BSideCMPA = (PWMCountMaxAF - PISigValue)/4096;  // = x1 - 4*8*128
  BSideCMPB = PWMCountMax   - BSideCMPA;          // = x4
  EPwm1Regs.CMPA.half.CMPA = ASideCMPA;   //A side CMPA
  EPwm1Regs.CMPB           = ASideCMPB;   //A side CMPB
```

Figure B.1. First part of the interrupt routine.

```
EPwm2Regs.CMPA.half.CMPA = ASideCMPA;   //Complementary
EPwm2Regs.CMPB           = ASideCMPB;   //Complementary
EPwm4Regs.CMPA.half.CMPA = BSideCMPA;   //B side CMPA
EPwm4Regs.CMPB           = BSideCMPB;   //B side CMPB
EPwm3Regs.CMPA.half.CMPA = BSideCMPA;   //B side low
EPwm3Regs.CMPB           = BSideCMPB;   //B side low
TableIndex++;
RampIndex++;
TextIndex++;
if(TableIndex==20){
  TableIndex = 0;
}
if(RampIndex==400){
  RampIndex = -400;
}
if(TextIndex==800){
  TextIndex = 0;
}
SigValueRef = LookUpTable[TableIndex] + (RampIndex*2);
if(SigValueRef<0){
  //AdcRegs.ADCTRL2.bit.SOC_SEQ2   = 0;
  EPwm5Regs.ETPS.bit.SOCAPRD       = 0;
  EPwm5Regs.ETSEL.bit.SOCAEN       = 0;
  AdcRegs.ADCTRL2.bit.INT_ENA_SEQ1 = 0;
```

Figure B.2. Second part of the interrupt routine.

```
    EPwm5Regs.ETSEL.bit.SOCBEN       = 1;
    EPwm5Regs.ETCLR.bit.SOCB         = 1;
    EPwm5Regs.ETPS.bit.SOCBPRD       = 1;
    AdcRegs.ADCTRL2.bit.SOC_SEQ2     = 0;
    AdcRegs.ADCTRL2.bit.INT_ENA_SEQ2 = 1;
  }else{
    //AdcRegs.ADCTRL2.bit.SOC_SEQ1 = 0;
    EPwm5Regs.ETPS.bit.SOCBPRD       = 0;
    EPwm5Regs.ETSEL.bit.SOCBEN       = 0;
    AdcRegs.ADCTRL2.bit.INT_ENA_SEQ2 = 0;
    EPwm5Regs.ETSEL.bit.SOCAEN       = 1;
    EPwm5Regs.ETCLR.bit.SOCA         = 1;
    EPwm5Regs.ETPS.bit.SOCAPRD       = 1;
    AdcRegs.ADCTRL2.bit.SOC_SEQ1     = 0;
    AdcRegs.ADCTRL2.bit.INT_ENA_SEQ1 = 1;
  }
  IntegralInPrev = IntegralIn;
  PIErrorPrev    = PIError;
  //Reinitialize for next ADC sequence
  AdcRegs.ADCTRL2.bit.RST_SEQ1   = 1;       // Reset SEQ1
  AdcRegs.ADCST.bit.INT_SEQ1_CLR = 1;       // Clear INT SEQ1 bit
  AdcRegs.ADCTRL2.bit.RST_SEQ2   = 1;       // Reset SEQ2
  AdcRegs.ADCST.bit.INT_SEQ2_CLR = 1;       // Clear INT SEQ2 bit
  //Acknowledge interrupt to PIE
  PieCtrlRegs.PIEACK.all = PIEACK_GROUP1;
  PieCtrlRegs.PIEIER1.bit.INTx6 = 1;
  return;
}
```

Figure B.3. Third part of the interrupt routine.

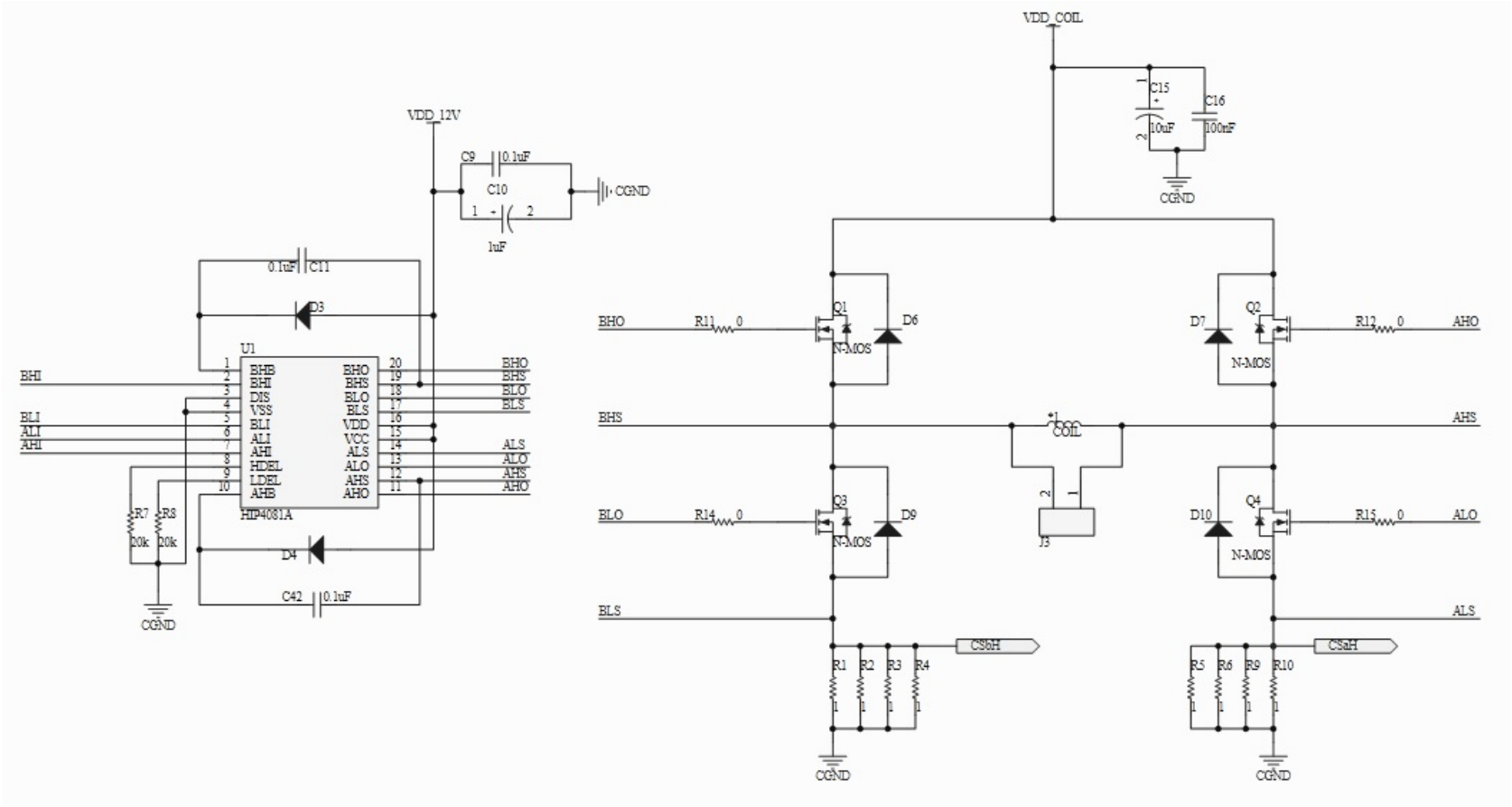

Figure B.4. Power inverter schematic.

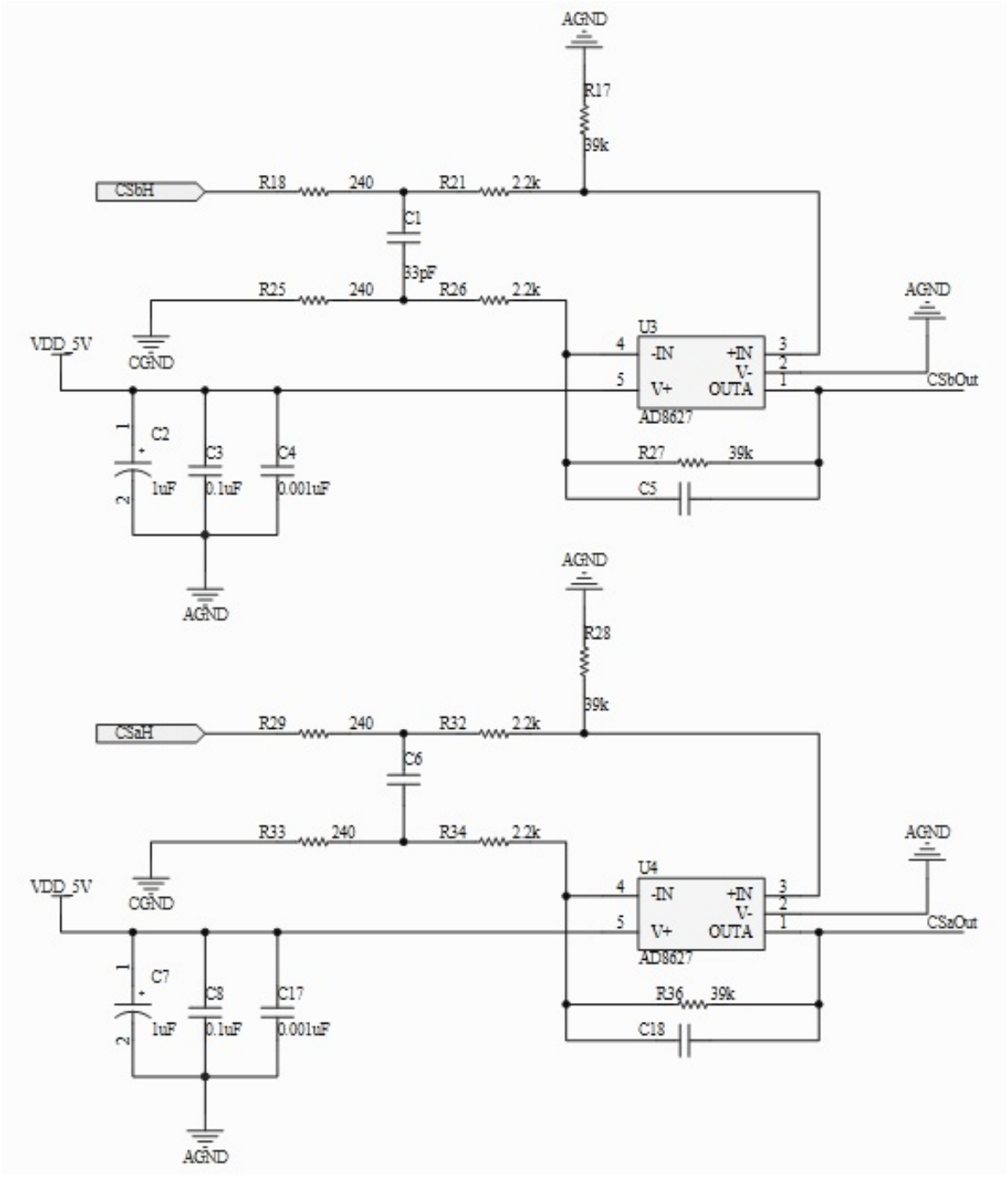

Figure B.5. Current sense circuitry schematic.

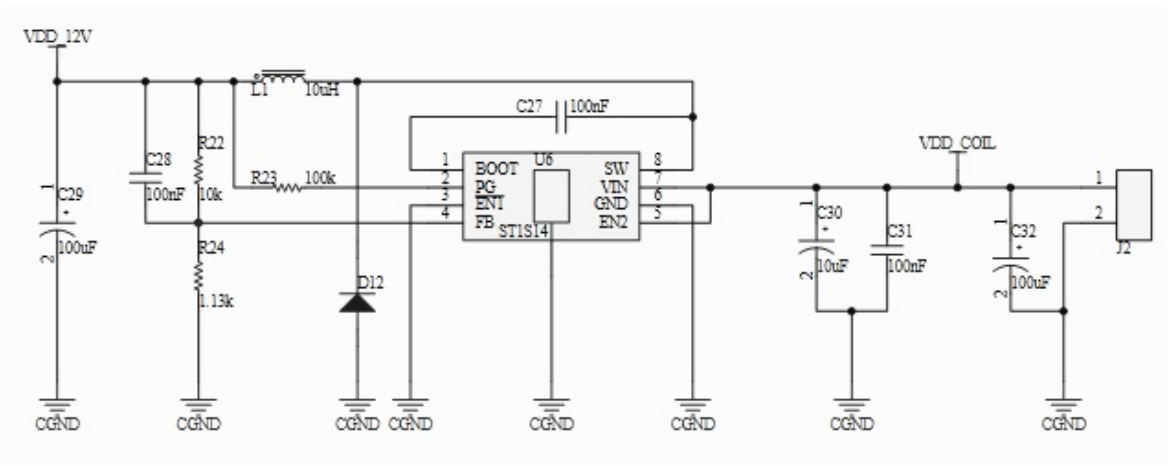

Figure B.6. Power supply schematic.

REFERENCES

1. *TMS320C2000 Experimenter Kit Overview*, Technical Report, Texas Instruments, Dallas, 2008.

2. Ohtuka, Y., H. Nishikawa, T. Koumura and T. Hattori, "2-Dimensional Optical Scanner Applying a Torsional Resonator with 2 Degrees of Freedom", *Proceedings of the 1995 IEEE International Conference on Micro Electro Mechanical Systems*, p. 306, 1995.

3. Lin, H. Y. and W. Fang, "A Rib-Reinforced Micro Torsional Mirror Driven by Electrostatic Torque Generators", *Journal of Sensors and Actuators*, Vol. 105, pp. 1–9, 2003.

4. Kwon, S., V. Milanovic and L. P. Lee, "A High Aspect Ratio 2D Gimbaled Microscanner with Large Static Rotation", *Proceedings of the 2002 IEEE/LEOS International Conference on Optical MEMs*, pp. 149–150, 2002.

5. Schweizer, S., S. Calmes, M. Laudon and P. Renaud, "Thermally Actuated Optical Microscanner with Large Angle and Low Consumption", *Journal of Sensors and Actuators*, Vol. 76, No. 1-3, pp. 470–477, 1999.

6. Sasaki, M., T. Yamaguchi, J. H. Song, K. Hane, M. Hara and K. Hori, "Optical Scanner on a Three-Dimensional Microoptical Bench", *Journal of Lightwave Technology*, Vol. 21, No. 3, pp. 602–608, 2003.

7. Lina, W. M., A. Schrothc, S. Matsumotoa, C. Lee and R. Maedaa, "Two-Dimensional Microscanner Actuated by PZT Thin Film", *Proceedings of the 1999 SPIE International Conference on Device and Process Technologies for MEMS and Microelectronics*, Vol. 3892, p. 133, 1999.

8. Motamedi, M. (Editor), *Micro-Opto-Electro-Mechanical Systems*, The Interna-

tional Society for Optical Engineering Press, Washington, 2005.

9. Gokdel, Y., B. Sarioglu, S. Mutlu and A. D. Yalcinkaya, "Design and Fabrication of Two-axis Micromachined Steel Scanners", *Journal of Micromechanics and Microengineering*, Vol. 19, No. 7, p. 075001, 2009.

10. Bernstein, J., W. Taylor, J. Brazzle, C. Corcoran, G. Kirkos, J. Odhner, A. Pareek, M. Waelti and M. Zai, "Electromagnetically Actuated Mirror Arrays for Use in 3-D Optical Switching Applications", *Journal of Microelectromechanical Systems*, Vol. 13, No. 3, pp. 526–535, 2004.

11. Okano, Y. and Y. Hirabayashi, "Magnetically Actuated Micromirror and Measurement System for Motion Characteristics Using Specular Reflection", *IEEE Journal of Selected Topics in Quantum Electronics*, Vol. 8, No. 1, pp. 19–25, 2002.

12. Houlet, L., P. Helin, T. Bourouina, G. Reyne, E.D.Gergam and H. Fujita, "Movable Vertical Mirror Arrays for Optical Microswitch Matrixes and Their Electromagnetic Actuation", *IEEE Journal of Selected Topics in Quantum Electronics*, Vol. 8, No. 1, pp. 58–63, 2002.

13. Usta, B. K., *Two-dimensional Selectively Thinned Steel Micromirrors*, M.S. Thesis, Boğaziçi University, Istanbul, 2011.

14. Kazmierkowski, M. and L. Malesani, "Current Control Techniques for Three-Phase Voltage-Source PWM Converters: A Survey", *IEEE Transactions on Industrial Electronics*, Vol. 45, No. 5, pp. 691–703, 1998.

15. Brod, D. M. and D. W. Novotny, "Current Control of VSI-PWM Inverters", *IEEE Transactions on Industry Applications*, Vol. IA-21, No. 3, pp. 562–570, 1985.

16. Malesani, L. and P. Tomasin, "PWM Current Control Techniques of Voltage Source Converters: A Survey", *Proceedings of the 1993 IECON International Conference on Industrial Electronics, Control, and Instrumentation*, Vol. 2, pp.

670–675, 1993.

17. Plunkett, A. B., "A Current Controlled PWM Transistor Inverted Drive", *Proceedings of the 1979 IEEE International Accounting Standards Annual Meeting*, pp. 785–792, 1979.

18. Kojabadi, H., B. Yu, I. Gadoura, L. Chang and M. Ghribi, "A Novel DSP-Based Current-Controlled PWM Strategy for Single Phase Grid Connected Inverters", *IEEE Transactions on Power Electronics*, Vol. 21, No. 4, pp. 985–993, 2006.

19. Holmes, D. and D. Martin, "Implementation of a Direct Digital Predictive Current Controller for Single and Three Phase Voltage Source Inverters", *Conference Record of the 1996 IEEE Industry Applications Annual Meeting*, Vol. 2, pp. 906–913, 1996.

20. Forghani Zadeh, H. and G. R. Mora, "Current-Sensing Techniques for DC-DC Converters", *Proceedings of the 2002 MWSCAS Symposium on Circuits and Systems*, Vol. 2, pp. 577–580, 2002.

21. Regan, T., *Application Note 105: Current Sense Circuit Collection*, Technical Report, Linear Technology, Milpitas, 2005.

22. Mohan, N., T. Undeland and W. Robbins, *Power Electronics: Converters, Applications, and Design*, John Wiley & Sons, Inc., Minnesota, 1995.

23. Ohm, D. and R. Oleksuk, "Influence of PWM Schemes and Commutation Methods for DC and Brushless Motors and Drives", *Proceedings of the 2002 P.E. Technology Conference*, 2002.

24. Shao, R., Z. Guo and L. Chang, "A PWM Strategy for Acoustic Noise Reduction for Grid-Connected Single-Phase Inverters", *Proceedings of the 2007 IEEE/APEC International Conference on Applied Power Electronics*, pp. 301–305, 2007.

25. *TMS320F2808 Digital Signal Processor Data Manual*, Technical Report, Texas Instruments, Dallas, 2003.

26. *TMS320C2000 Experimenter's Kit Schematic, Release 2.0*, Technical Report, Texas Instruments, Dallas, 2008.